Journal of South American Earth Sciences 110 (2021) 103364

Contents lists available at ScienceDirect

Journal of South American Earth Sciences

journal homepage: www.elsevier.com/locate/jsames

The Archean Pavas Block in Uruguay: Extension and tectonic evolution based on LA-ICP-MS U–Pb ages and airborne geophysics

Henri Masquelin [a,*], Tahar Aïfa [b], Fernando Scaglia [c], Miguel A.S. Basei [d]

[a] Instituto de Ciencias Geológicas, Facultad de Ciencias – UdelaR, Iguá 4225 P12 Ala sur, 11400, Montevideo, Uruguay
[b] Univ. Rennes, CNRS, Géosciences Rennes – UMR6118, Campus Beaulieu, 35042, Rennes, France
[c] Post-graduate Course, PEDECIBA Geosciences, Uruguay
[d] Centro de Pesquisas Geocronológicas, Universidade de São Paulo, Brazil

ARTICLE INFO

Keywords:
Precambrian
Zircon texture
Granitic gneiss
Nico Pérez Terrane
Gamma spectrometry

ABSTRACT

The Pavas Block is an Archean/Paleoproterozoic inlier located in the central segment of Uruguay's Precambrian exposition. A new insight initiated due to the acquisition of airborne geophysical data and new U–Pb zircon dating. The correlation of Archean crustal inliers in the amalgamation of the South American Platform is one of the main objectives in the Precambrian geological investigation. Although Ediacaran lateral strike-slip shear zones controlled the Pavas Block, their ultimate boundaries are not clear. Furthermore, a pre-Neoproterozoic metasedimentary succession discordant on this block is often confused with Neoproterozoic ones. Correctly identifying these limits is a necessary task to modify wrong tectono-stratigraphic models. The airborne total count radiometric imaging and the horizontal derivative of the total magnetic field anomaly reduced to the pole at 1000 m elevation led to establishing the Pavas Block's dimensions, based on new structural interpretation. The filtered magnetic anomaly is concordant with the previous Bouguer anomaly indicating a westward virgation of the Pavas Block in the north. This inlier narrows through the Minas city and along the Sarandí del Yí shear zone. The Sierra de Sosa and Sierra Ballena shear zones were confirmed as lateral limits. The total count radiometric map highlights the presence of brittle-fault reactivation. The Archean La China Complex containing zircons from three periods (~3.3–3.1 Ga; 3.0; 2.8–2.7 Ga) is in the Pavas Block's centre. New U–Pb zircon geochronology provided six samples from different metagranitoids that yielded LA-ICPMS U–Pb zircon ages ranging between 3353 ± 9 Ma and 1839 ± 2 Ma. Its southern periphery shows more recent Archean and Orosirian metagranitoids. These rocks were later partially affected by Neoproterozoic deformation. The preservation of igneous textures, field relationships, and zircon textures suggested that younger Neoarchean intrusive granitoids emplaced within the basal granitic gneiss "La China" complex. The pre-Neoproterozoic metasedimentary cover intercalates with Neoproterozoic successions until the southern end of the Pavas Block against the Sarandí del Yí Shear Zone. Finally, one granitoid devoid of Archean inherited zircons yielded a concordant $^{207}Pb/^{206}Pb$ zircon age of 1999 ± 3 Ma (MSWD = 8.1) interpreted as magmatic crystallisation. This Orosirian K-feldspar granite is likely to set the southern border of the block in a transitional crust. The Pavas Block is limited from the Villa Serrana Block by a schist belt of Mesoproterozoic protoliths, and reports enough information to be interpreted as a suspect terrane.

1. Introduction

The Pavas Block is a small (i.e., 3000 km^2), elongated Archean/Paleoproterozoic inlier located in the centre of the Nico Pérez Terrane of central Uruguay (Preciozzi et al., 1979, 1985; Masquelin, 2006; Sánchez Bettucci et al., 2010; Oriolo et al., 2016a; Oyhantçabal et al., 2018, Fig. 1). The Nico Pérez Terrane (NPT) of Uruguay is part of the West-Gondwana Neoproterozoic amalgamation (Brito Neves et al., 1999; Campos Neto, 2000). This crustal segment forms an acute triangle, limited to the eastern Rio de la Plata Craton by the Sarandí del Yí shear zone and the western terrane by the Sierra Ballena Shear Zone (Bossi and Campal, 1992; Oyhantçabal et al., 1993; Oriolo et al., 2016a, b).

The definition of minor entities like the Cerro Chato and Pavas subterranes (Oyhantçabal et al., 2018) or blocks (Oriolo et al., 2019) is not new (e.g., Preciozzi et al., 1979; Masquelin, 2006). However, this scheme provides new insight into the structural framework of the

* Corresponding author.
E-mail addresses: emasquelin@fcien.edu.uy, enrique.masquelin@pedeciba.edu.uy (H. Masquelin).

https://doi.org/10.1016/j.jsames.2021.103364
Received 27 July 2020; Received in revised form 31 March 2021; Accepted 27 April 2021
Available online 24 May 2021

Precambrian in central Uruguay in the light of new geochronological and geophysical data. So far, the Pavas Block is the only one exposing Archean rocks in the NPT (Hartmann et al., 2001; Mallmann et al., 2007). However, the isotopic inheritance reveals that Archean sources are widespread in the whole Nico Pérez Terrane (Oyhantçabal et al., 2018). Archean inheritance was verified in the TDM model ages Sm–Nd and Lu–Hf in zircon (Babinski et al., 1997; Hartmann et al., 1999; Santos et al., 2003; Mallmann et al., 2007; Oyhantçabal et al., 2011, 2018, 2018; Oriolo et al., 2015, 2016a, 2016a; Lara et al., 2020). Likewise, the metamorphic zircons show a U–Pb system that registers robust Archean inheritance in all the analyses (Hartmann et al., 2001; Gaucher et al., 2011; Oyhantçabal et al., 2012; Oriolo et al., 2019). The detrital provenance of the metamorphic cover succession shows Archean age peaks that strongly contrast with the ages of the Rio de la Plata Craton (Blanco et al., 2009; Peçoits et al., 2016; Oyhantçabal et al., 2021).

The Pavas Block's extension is of principal interest due to the suspicion of a terrane accretion model to test a theory presented in some recent works (Rapela et al., 2011; Girelli et al., 2018). The whole NPT was initially interpreted as a Neoproterozoic tectonostratigraphic "suspected" terrane separated through ductile shear zones (Bossi and Gaucher, 2004). Ambiguity revolves around whether the tectonic events responsible for the updated structural framework reflect intra-plate (intra-cratonic) processes or those linked to and driven by interactions at plate margins (e.g., Clark et al., 2007). The primary character of crustal blocks in an orogenic collage must distinguish itself from their late-orogenic secondary framework (Şengör and Dewey, 1990; Fernandes et al., 1995; De Toni et al., 2021). Tectonic models of Precambrian orogens either miss the existence of large brittle faults or mistake them for ductile shear zones. The inaccuracies in the description of lithostratigraphic terranes or blocks apply to the NPT. Therefore, the structural analysis needs to point towards definitions of different meanings. High-resolution airborne geophysics would make it possible to underpin these definitions. Likewise, high-accuracy airborne magnetic and radiometric data is a powerful tool for scrutinising brittle faults and their kinematic indicators.

The Pavas and Cerro Chato Blocks represent the western foreland basement of the Dom Feliciano Belt (DFB; Basei et al., 2000; Masquelin, 2006; Sánchez-Bettucci et al., 2010; Oyhantçabal et al., 2011; Philipp et al., 2016; Peel et al., 2018; Hueck et al., 2018; Oriolo et al., 2019). A curved discontinuity called the Sierra de Sosa Transcurrent System separated both blocks (Campal and Schipilov, 1999; Bossi et al., 2001). The discontinuity is also known as the Cueva del Tigre or Sierra de Sosa strike-slip shear zone (Masquelin, 2006; Gaucher et al., 2014a; Oyhantçabal et al., 2018).

The Pavas Block is made up of a basal granitic gneiss, probably derived from magmatic TTG Suites, and a medium to high-grade metamorphic cover sequence (Hartmann et al., 2001). One question that arises is to quantify the full exposition of the Archean rocks and their boundaries, especially through its southern edge, and its relationship with the southernmost Villa Serrana Block (Bossi and Gaucher,

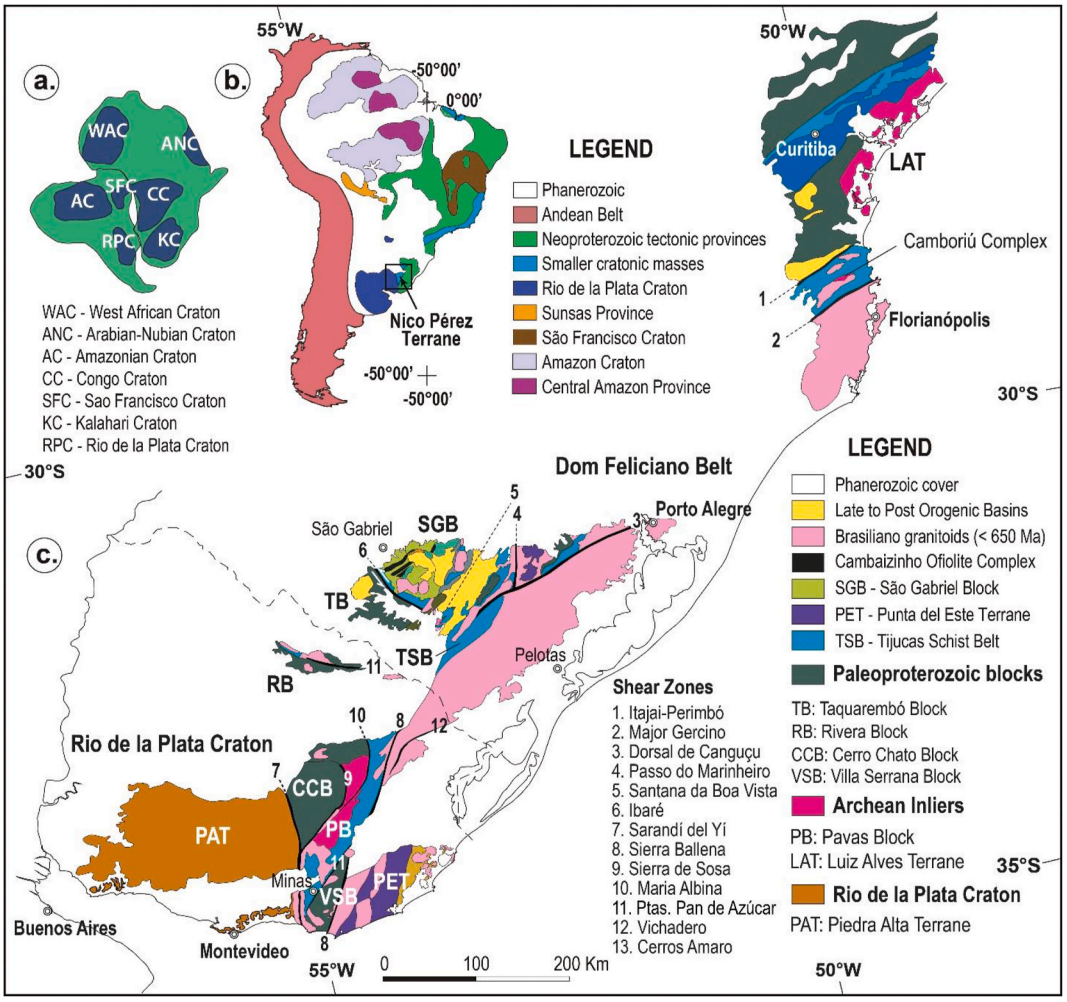

Fig. 1. Geotectonic map: a) Location of South American cratons (Modify from Fernandes et al., 1995), b) Location of Mantiqueira Province and study area in Southwestern Gondwana (Modify from Sato et al., 2003), c) Relative setting of the Cerro Chato, Pavas and Villa Serrana Blocks between the Dom Feliciano Belt and the Rio de la Plata Craton (Modify from Preciozzi et al., 1985).

2004).

Another question concerns the different degrees of tectono-thermal recycling of the Archean crust and the geological records that are evidencing a Rhyacian-Orosirian multi-episodic tectonic evolution (Oyhantçabal et al., 2012, 2018). The lithological correlation between the Pavas Block and the Congo-São Francisco Craton can help the geotectonic reconstructions concerning the geology of the pre-Neoproterozoic cover sequence, named the Las Tetas Complex (Hartmann et al., 2001). Locally, the Las Tetas Complex indicates a much broader and interspersed distribution towards the south (until the Minas city). The São Francisco Craton reported another metamorphic association composed of oligomictic quartz-conglomerates, fuchsite--sillimanite quartzites, amphibolites, micaschists, stromatolitic carbonatic rocks, and BIF (Oliveira et al., 2002; Milési et al., 2002; Rosière et al., 2018). Chromium-rich hydrothermalism that altered Pre-Neoproterozoic rocks is common in many cratonic regions worldwide (e.g., Nutman et al., 2014; Singh and Slabunov, 2016; Kielman et al., 2018; Albert et al., 2018). Together with their isotopic fingerprints or signatures (Scherer et al., 2007; Harley et al., 2007; Pearce, 2014; Grimes et al., 2015; Roberts and Spencer, 2015), they could be a powerful tool to make correlations like those pointing to the Columbia Paleo-continent's reconstructions (e.g., Girelli et al., 2018; Bruno et al., 2021).

This study aims to revise the Pavas Block's extension towards the south and its lateral boundaries. This work attempts to (i) discuss their boundaries, using airborne magnetic and total count radiometric data, and (ii) discriminate Archean-recycled to non-recycled rocks. For this purpose, we have used the U–Pb age correlation from six new laser ablation ICP-MS U–Pb zircon analyses. Zircon textural features and petrography are essential tools to contextualise geochronological data. All zircons studied come from high-to-medium grade metamorphic rocks of the La China Complex (Hartmann et al., 2001) and the Campanero Unit (Sánchez Bettucci et al., 2003).

2. Geological setting

2.1. Local setting and boundaries of the Pavas Block

The discovery of the "Pavas Formation" initiated as a photointerpretation recognising contrasted geomorphology and lithological associations (Preciozzi et al., 1979). The exposing area is located between the Sierra de Sosa and the María Albina shear zones (Bates et al., 2016; Oriolo et al., 2016a; Sánchez Bettucci et al., 2021). The block has been mapped as a narrow band of 20 km wide and 200 km in length on average (most extensive to the North: 32 km), oriented NE-SW between latitudes −33.78° and −32.80° (Fig. 1c) (Preciozzi et al., 1985; Gaucher et al., 2014a; Oriolo et al., 2019). The revised Bouguer anomaly map of Uruguay (Rodríguez et al., 2015) shows a critical positive anomaly at the north-eastern corner of this area. The magnetotelluric profile indicates that the Pavas and Cerro Chato blocks both have a 200 km's thickness, which is inherited from a cratonic setting (Bologna et al., 2019). In geological maps, the block's shape seems controversial, depending on how different authors interpreted their boundary faults (e.g., Preciozzi et al., 1979; Sánchez Bettucci et al., 2010; Oyhantçabal et al., 2021). Some sketches place an eastward convexity for the western limit, called the Cueva del Tigre Fault (Preciozzi et al., 1979). Others

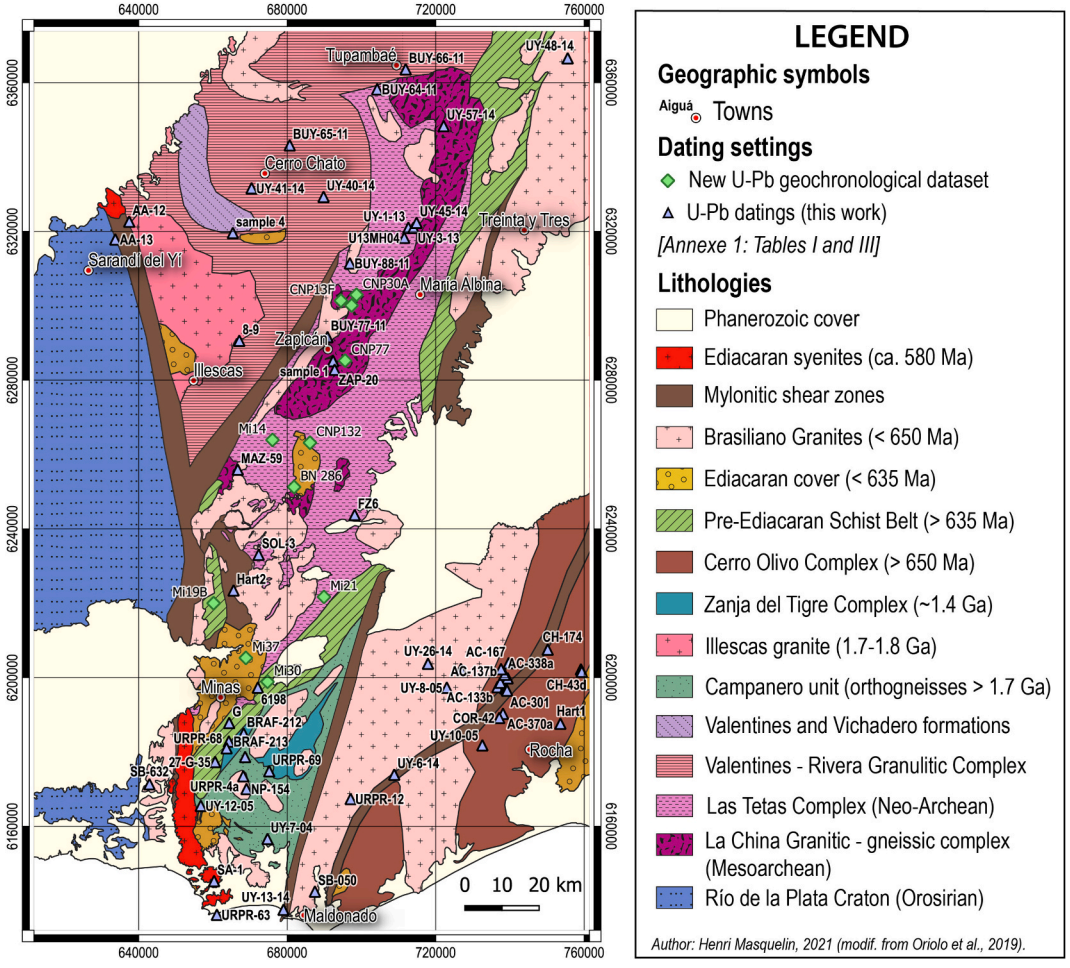

Fig. 2. Regional Geological sketch of the Nico Pérez Terrane, showing the main structural features and lithological units (Modify from Oriolo et al., 2019).

place a westward convexity, giving the block a spindle shape (e.g., Bossi et al., 2001; Mallmann et al., 2007; Sánchez Bettucci et al., 2010). The Tupambaé shear zone is its northern limit (Bates et al., 2016). Southward, the NW-SE striking Santa Lucia granite truncated it. Eastward, it limits through the Puntas de Pan de Azúcar shear zone (Guerrero, 2016) and the Sierra Ballena shear zone as the last resort (Hartmann et al., 2001). This definition mostly concerns the basal granitic-gneissic complex because many "flakes" of the Neoarchean metamorphic cover succession extend beyond the contact of the inner granitic-gneissic nucleus (Fig. 2) (e.g., Oriolo et al., 2016a; Oyhantçabal et al., 2021). Most interpretations have in common that the Sierra de Sosa shear zone represents the western boundary (Campal and Schipilov, 1999; Bates et al., 2016; Oriolo et al., 2016a). Many geologic maps place thrusts dipping to the NW, others to the SE, but none present structural measurements at the 1:500,000 scale to sustain this information.

2.2. Geotectonic location

The Archean block is in the central segment of the Precambrian exposition in Uruguay called the "Nico Pérez Terrane" (NPT; Bossi and Campal, 1991, 1992; Oriolo et al., 2016a, Fig. 1). The NPT locates between the Rio de la Plata Craton (Almeida et al., 1973) and the Aiguá - Pelotas Batholith (Masquelin, 2006). Together with the DFB, this tectonic wedge represents part of the Brasiliano orogenic collage (e.g., Şengör and Dewey, 1990) named the Mantiqueira Province in Brazil (Hasui, 1982; Jost and Hartmann, 1984; Da Silva et al., 2005). This part of the South American Platform includes many inliers of different ages and histories, which took place in Late Proterozoic times (Brito Neves and Cordani, 1991; Campos Neto, 2000; Brito Neves et al., 2014). The Mantiqueira province was already known as having an "Archean structure" and a Proterozoic evolution that combined two terranes' kinds, (i) granulitic and (ii) granitic-gneissic with supracrustal relics (Hasui, 1982). Some inliers are cratonic, and others are "fertilised" (Bologna et al., 2019). The final structure developed after a protracted Neoproterozoic amalgamation of major crustal blocks and branched systems of orogenic belts (Brito Neves et al., 2014). It gave rise to the Western Gondwana accretion after the Rodinia breakup (Cordani et al., 2003). Furthermore, the Pavas Block also represents basement rocks involved in the foreland of the Neoproterozoic Dom Feliciano Belt (DFB; Fragoso Cesar, 1980; Fernandes et al., 1995; Basei et al., 2000; Oyhantçabal et al., 2009, 2018; Oriolo et al., 2016a, c; Hueck et al., 2018; Masquelin et al., 2017; Lara et al., 2020). These basement rocks were affected by Neoproterozoic metamorphism, deformation, and granitic magmatism (Oriolo et al., 2016a, c; Hueck et al., 2018). The degree of recycling is variable depending on each block. The DFB has been correlated with the Kaoko and Gariep Belts of southwestern Africa. All of them show a similar tectono-magmatic evolution during the Pan-African/Brasiliano orogenesis (Basei et al., 2008; Goscombe and Gray, 2007; Frimmel et al., 2011; Hueck et al., 2018 and references therein).

2.3. Geotectonic evolution

The juxtaposition of the Río de la Plata, Kalahari, and Congo Cratons together with other continental fragments such as the Pavas Block and the Luiz Alves Terrane took place to form the Western Gondwana (Basei et al., 2005; Goscombe et al., 2005; Gray et al., 2008). The first cause of structural complexity in the Mantiqueira Province and the Dom Feliciano Belt (DFB) is that penetrative strike-slip shear zones usually juxtapose sectors with no connection in the transversal section (e.g., Burke and Şengör, 1986). The last Neoproterozoic tectonic event, associated with the Sierra Ballena strike-slip shear zone, was transpressive (Oyhantçabal et al., 2009, 2011; Oriolo et al., 2016b). It was probably followed by lateral escape, although the "indentor" is not clear (Fernandes et al., 1993; Tommasi et al., 1994). The Neoproterozoic magmatic activity in the NPT included the last emplacement of late-orogenic granites (~600-580 Ma), channelizing through shear zones (e.g., Fort, 2020; Lara et al., 2020). The Pavas Block can be considered an inlier that survived from both the Paleoproterozoic recycling and the Brasiliano/Pan-African tectono-thermal event. Therefore, the whole NPT was postulated as a Congo Craton fragment (Oriolo et al., 2016a; Oyhantçabal et al., 2018).

An integrated tectonic evolution suggests that NPT's Archean crust underwent magmatic accretion and recycling during Rhyacian and Orosirian tectono-metamorphic events (Santos et al., 2003; Oyhantçabal et al., 2012). The Rhyacian event recorded magmatism at ca. 2.2–2.1 Ga followed by high-grade metamorphism associated with crustal anatexis at ca. 2.1–2.0 Ga (Oyhantçabal et al., 2012; Oriolo et al., 2016a; Girelli et al., 2018). This first amalgamation underwent a polyphase deformation during the collision between the Kalahari and the Congo-Rio de la Plata plates in the interval 650-600 Ma (Fernandes et al., 1992; Oriolo et al., 2016a; Hueck et al., 2018). This protracted evolution could involve a suspected terrane accretion process (Rapela et al., 2011). In this case, amalgamation's driving mechanism is not obvious because the crustal growth might occur in an environment of long-term subduction and plate convergence without the collision of large continental blocks (Murphy and Nance, 1991; Cawood and Buchan, 2007).

2.4. Regional age constraints

Absolute age constraints presented here cover the entire Nico Pérez Terrane. Sm–Nd TDM model ages were treated in general. Such U–Pb in zircon combined with other methods) are treated in detail. The U–Pb samples are shown in the geological map (Fig. 2). Tables I and III displays all the U–Pb results, collected and antecedent (Annexe 1, Data-In-Brief).

2.4.1. Sm–Nd and Lu–Hf TDM-model ages

Although Sm–Nd and Lu–Hf TDM-model ages and zircon inheritance in NPT reflect dominant Paleoproterozoic sources, they also indicate the ubiquitous presence of an Archean precursor (Santos et al., 2003; Mallmann et al., 2007; Oyhantçabal et al., 2021; Oriolo et al., 2016a; Lara et al., 2020). Based on the TDM (Nd) and (Hf) model-ages, Oyhantçabal et al. (2012) suggested a polycyclic evolution initiating in the Archean. Southern Neoproterozoic granites (~596–610 Ma) of the Villa Serrana Block and the Aiguá Batholith (Fig. 2) gives an evolved Sr and Nd isotopic signatures ($^{87}Sr/^{86}Sr_i$ of 0.708; negative εNd of −14 to −20). An Nd-TDM model age is in the interval ~2.3–2.8 Ga. Their zircons yield a negative εHf(t) (−21 to −27) but Hf model ages of ~3.6 Ga (Lara et al., 2020). Archean inherited components also appear in the northern Neoproterozoic granites (~619 Ma). Zircons show Hf model ages of 2.69 and 2.59 Ga, respectively (Fort, 2020). Both results confirm Archean precursors' widespread occurrence westward along the Sierra Ballena Shear Zone (Oyhantçabal et al., 2018). In the Villa Serrana Block, the mylonitic syenogranite (sample NP-154; Table I, Annexe 1) shows an Nd-TDM of 2.84 Ga, indicating an Archean mantellic extraction for the source (Mallmann et al., 2007). Detrital zircon ages collected in metasediments of the Zanja del Tigre Complex yielded (i) Paleoproterozoic ages of 2.18 to 1.96 Ga, and (ii) Archean ages of 3.54 to 2.67 Ga (Mallmann et al., 2007).

2.4.2. Rhyacian/orosirian evolution based on the Th–U–Pb system

The complete Paleoproterozoic evolution is documented in Rivera and Cerro Chato blocks (Fig. 1c). Using combined geochronological methods, as SHRIMP U–Pb zircon, Th–U–Pb monazite (CHIME - EPMA method) and K–Ar (W-R and amphibole), the resulted evolution recorded (i) Rhyacian magmatism at 2.17–2.11 Ga, and (ii) Orosirian granulite-facies anatectic event, at ~2.08 Ma (on zircon overgrowths), and the metamorphic thermal peak at ~1.98 Ga in monazite (Oyhantçabal et al., 2012; Table III; Annexe 1).

Zircons extracted from metagranitoids of the Valentines region (Fig. 2) yielded U–Pb zircon (SHRIMP) ages of ~2.2 Ga. These zircons

show some Neoarchean (~2.7 Ga) inherited euhedral cores with oscillatory zoning (Santos et al., 2003; Oriolo et al., 2016a; Annexe 1: Table III). Oscillatory zoning pattern (OZP) is also present in the rims. Zircon cores yielded a weighted mean $^{206}Pb/^{238}U$ age of 2106 ± 21 Ma (MSWD of concordance = 3.2) interpreted as the igneous crystallisation age. Meanwhile, some rims yielded an age of ~600 Ma, interpreted as the Neoproterozoic metamorphism with anatexis (Santos et al., 2003; Table III, Annexe 1). The $^{207}Pb/^{206}Pb$ age of 2057.5 ± 2.8 Ma (MSWD = 0.96) (n = 6) was interpreted as the age of metamorphic recrystallisation. Unzoned overgrowth rims pointed to a granulite facies anatectic event (~2.0 Ga).

A Statherian tectono-thermal event was reported in the southernmost Villa Serrana Block. The Campanero Unit constitute the gneissic rocks of the Paleoproterozoic basement in this region (Sánchez Bettucci et al., 2003). A syenogranite (sample 6198; Table III, Annexe 1) yielded the first U–Pb conventional dating giving a Discordia upper intercept age of 1735 + 32/-17 Ma and interpreted as magmatic crystallisation. Meanwhile, the authors explained the lower intercept age (723 + 240/-210 Ma) as due to Neoproterozoic deformation. Meanwhile, they interpreted the 1754 ± 6.8 Ma upper intercept age as magmatic crystallisation. Granitic plutons of 1.8–1.7 Ga, like the Illescas granite in the Cerro Chato Block (Fig. 2), are typically post-orogenic concerning the Orosirian orogenesis (~2.0 Ga). Despite presenting a Brasiliano mylonitization, these granites were correlated with the Illescas granite based on their Rb–Sr and U–Pb age (Campal and Schipilov, 1995; Oriolo et al., 2019).

The Rhyacian/Orosirian evolution can be correlated with the Camboriú (Da Silva et al., 2005) and Santa Maria Chico complexes (Tickyj et al., 2004; Girelli et al., 2018), as both reported the ages mentioned above. Girelli et al. (2018) pointed out that the granulite facies metamorphic event at ~2.06 Ga was at the onset of multi-accretional terranes' amalgamation against the Rio de la Plata Craton (RPC).

2.4.3. Geochronology in the Pavas Block

The Pavas Block contains metagranitoids displaying Neo to Meso-Archean metamorphic ages obtained by the U–Pb zircon (SHRIMP) method (Hartmann et al., 2001; Gaucher et al., 2011). Hartmann et al. (2001) separated two events at 3.41–3.15 Ga (magmatism and recrystallisation) and 2.76 Ga (Pb-loss by deformation). The first dated orthogneiss yields zircon cores reaching a U–Pb SHRIMP age of 3404 ± 8 Ma (Hartmann et al., 2001). This age was interpreted as magmatic crystallisation. In contrast, slightly younger ages (~3.1 Ga) in the zircon rims were interpreted as partial resetting due to an upper amphibolite facies metamorphism. Gaucher et al. (2011) obtained a new U–Pb LA-ICP-MS zircon age of 3096 ± 45 Ma near the first dating place and interpreted it as partial melting crystallisation. Gaucher et al. (2014a) presented a new SHRIMP U–Pb zircon age from a mylonitic granitoid (sample FZ6; Table III, Annexe 1) that yielded a $^{207}Pb/^{206}Pb$ magmatic crystallisation age of 2787 ± 6 Ma. Hartmann et al. (2001) suggested that sectors having ~2.76 Ga were not affected by the Orosirian anatectic event (at ~2.07 Ga). On the other hand, the minimum age of the detrital zircon provenance in the Las Tetas Complex is 2717 ± 24 Ma (Hartmann et al., 2001). Oyhantçabal et al. (2021) confirmed that the Las Tetas Complex is characterized by the lack of Proterozoic detrital zircon grains. Following these authors, the absence of Rhyacian/Orosirian zircon grains is remarkable, despite this being the dominant age peak in all other units of the NPT. A ca. 630-600 Ma metamorphic overprints this complex, constrained by Ar/Ar phlogopite and muscovite data (Oriolo et al., 2016b). Neoproterozoic intrusions within the Pavas Block are represented by the Zapicán diorite that emplaced parallel to the Sierra de Sosa shear zone. This late-kinematic diorite yields a magmatic crystallisation age ($^{206}Pb/^{238}U$) of 610.4 ± 2.5 Ma (Oriolo et al., 2016a).

2.5. Main rock units and structures

The Pavas Block comprises the pre-Neoproterozoic La China Complex (Hartmann et al., 2001), as the basement unit, and the Las Tetas metasediments, as a platform cover (e.g., Preciozzi et al., 1979, 1985; Oyhantçabal and Vaz Chaves, 1990; Hartmann et al., 2001; Oriolo et al., 2016a; Masquelin et al., 2017; Oyhantçabal et al., 2021). The contact between both complexes is tectonic, including thrusts and high angle transcurrent shear zones (Campal and Schipilov, 1999; Hartmann et al., 2001; Bossi et al., 2001; Oriolo et al., 2016a).

2.5.1. The La China complex

The La China Complex contains felsic granitic-gneisses, amphibolites and ultramafic rocks generally retrogressed to actinolite-schists, talc-schists, and serpentinites (Preciozzi et al. 1979, 1985, 1985; Hartmann et al., 2001; Gaucher et al., 2014a; Oriolo et al., 2016a). A tonalite - trondhjemite - granodiorite (TTG) affinity was assumed for these migmatitic orthogneisses, although no geochemistry emerges (Hartmann et al., 2001; Gaucher et al., 2014a). The granitic gneisses recorded low angle layering and interspersed with amphibolites. However, L-fabrics and a penetrative mineral lineation represent it, plunging at a low-angle to the southwest or south (Oriolo et al., 2016b; Masquelin et al., 2017). The basal gneisses are variable under the Ediacaran Barriga Negra formation (Masquelin et al., 2017; Núñez Demarco et al., 2018a, b). A banded, fine-grained, muscovite-rich granitoid is common. Then it is crosscut first by white pegmatites and then by a K-feldspar rich coarse-grained granitoid. Other sections show a flat-lying mylonitic rock with a strong stretching lineation plunging towards the N-E. Low angle contact relationships with the stretched meta-conglomerate, stratified sericite-schists and quartzites are visible (Núñez Demarco et al., 2018b).

2.5.2. The Las Tetas Complex

The Las Tetas Complex is a medium-grade metamorphic succession composed of fuchsite-bearing meta-conglomerates, quartzites, garnet - biotite micaschists, quartz-(tourmaline)-mica schists, marbles, black-shales, BIF, garnet-bearing and garnet-free amphibolites (Oyhantçabal and Vaz Chaves, 1990; Preciozzi et al., 1988a, b; Hartmann et al., 2001; Gaucher et al., 2014b; Masquelin et al., 2017; Oyhantçabal et al., 2021). In recent geological maps, this succession extends over the granitic-gneissic basement to the SBSZ (Oriolo et al., 2019; Oyhantçabal et al., 2021). Sillimanite-bearing quartzites were described in the north (Oyhantçabal and Vaz Chaves, 1990), whereas staurolite-garnet micaschists were described in the south (Preciozzi et al., 1989; Hartmann et al., 2001). Quartz-mica schists, quartzites and fuchsite-bearing meta-conglomerates are interbedded and affected by upright folds (Oriolo et al., 2016b). Chevron folds and kinks are common. Although no detrital zircons are available on stromatolitic carbonate successions, field relationships suggest that these carbonates associate with the rest of the above-mentioned rocks. The youngest detrital zircon age peak (n = 16) of ~2764 Ma still constrains the maximum deposition age of Las Tetas' succession (Hartmann et al., 2001; Oyhantçabal et al., 2021). A Neoarchean/Siderian deposition age is likely because detrital zircons from the whole Proterozoic provenance are lack (Oyhantçabal et al., 2021). This top provenance age is reinforced given the Orosirian age of the isotropic Arroyo Perdido granite (near Minas), which crosscut the Las Tetas Complex. This granite yielded an Rb–Sr age of 2001 ± 117 Ma (Umpierre and Halpern, 1971; Gaucher et al., 2006), which were confirmed at 2036 ± 4 Ma by U–Pb SHRIMP method (Gaucher et al., 2014b). The minimum age of recycling was constrained by a $^{40}Ar/^{39}Ar$ age of 621.4 ± 1.0 Ma in phlogopite taken from the Polanco marbles (Oriolo et al., 2016b).

Its original basin could be a stable-shelf siliciclastic-carbonate platform (Hartmann et al., 2001). The Las Tetas Complex is thrust-stacked and interspersed with the La China Complex rocks (Hartmann et al., 2001; Gaucher et al., 2014b). Sillimanite indicates high-grade metamorphic/anatectic conditions above 600 °C (Oyhantçabal and Vaz

Chaves, 1990). The stretching lineation on quartz-clasts of the basal fuchsite-bearing meta-conglomerate is 15°/160° (Masquelin et al., 2017; Núñez Demarco, 2018a, b; 2019). Despite the N–S stretching, the meta-conglomerate still preserves bedding (Masquelin et al., 2017). The Polanco/Manguera Azul marbles also show mineral lineations (15°/220°) and mineral assemblages coherent with upper greenschist facies (Silva Lara et al., 2018).

2.5.3. Sierra de sosa shear zone (SSSZ)

The Sierra de Sosa shear zone separates the Cerro Chato from the Pavas block. Campal and Schipilov (1999) defined first the "Sierra de Sosa Transcurrent System". This system involved strike-slip faults and thrusts. The Sierra de Sosa Shear Zone (SSSZ) (Gaucher et al., 2014a) crosscut different lithologies and presents a mean mylonitic foliation of 219°/70° and a mean stretching lineation of 15°/225° (Oriolo et al., 2016b). The "transcurrent system" is made up of a 3–5 km wide strip, with a 020° orientation that extends over tens of kilometres in length. Kilometre-wide protomylonitic Kfs-rich granitoids and vertical mylonites are the main rocks (Campal and Schipilov, 1999). However, it also contains layered gneisses and amphibolites. This lithological association suggests that initial conditions during the deformation were linked to amphibolite facies. The mylonites contain "shreds" of carbonate rocks, green schists, and BIF (Campal and Schipilov, 1999). Different authors recognise the dextral strike-slip at different scales (Bossi et al., 2001; Masquelin et al., 2017). However, mesoscopic kinematic indicators like S–C shear bands and δ- and σ-type feldspar mantled porphyroclasts indicate a sinistral shear (Oriolo et al., 2016b). The SSSZ encounters the SYSZ at its southwestern limit. The Sierra de Sosa Shear Zone hosts protomylonitic K-feldspar granites to the west. Finally, the SSSZ hosts the 030° striking, late-kinematic intrusion of the Zapicán diorite, which yields a U–Pb zircon age of 610 ± 10.5 Ma (Oriolo et al., 2016a, b).

2.5.4. Maria Albina Shear Zone (MASZ)

The NE-SW trending "Fraile Muerto - Maria Albina Shear Zone" (MASZ) (Sánchez Bettucci et al., 2021; Oriolo et al., 2016b) along the eastern border of the Pavas Block has been first considered the limit with the DFB (e.g., Preciozzi et al., 1979). This shear zone shows a thrust-imbrication between the granitic gneisses and the Las Tetas Complex supracrustal rocks (Oriolo et al., 2016a).

2.5.5. The Tupambaé Shear Zone

The Tupambaé Shear Zone (Sánchez Bettucci et al., 2021) shows granitic mylonites. Kinematic indicators like foliation-fish and σ-type feldspar mantled porphyroclasts with tensional microfractures exhibit a dextral shear (Oriolo et al., 2016b). The mylonites recorded a secondary paragenesis of fine-grained biotite, epidote, and sericite, characterising retrogressive metamorphic conditions. Y and P shears indicate a dextral shearing under brittle conditions (Oriolo et al., 2016b).

2.5.6. Neoproterozoic metasediments and volcanic rocks

There are sedimentary successions in the NPT that constitute small, elongated, erosive relics formed by syn-orogenic deposits of "molassic" nature (Fambrini et al., 2005; Masquelin, 2006). The Yerbal formation (Gaucher, 2000; Blanco et al., 2009; Hueck et al., 2018) is another Ediacaran turbidite that erosive superimposes the La China Complex. It shows a detrital zircon provenance indicating a Cryogenian to Tonian maximum deposition age (Oyhantçabal et al., 2021). A deformation event separates the Yerbal formation from the Barriga Negra formation. Ages between ca. 3.4 and 2.7 Ga are common in detrital zircons from the conglomerates and sandstones of the Barriga Negra Formation (Blanco et al., 2009; Peçoits et al., 2016; Oyhantçabal et al., 2021). The La China and Las Tetas complexes provided large boulders of muscovite-rich orthogneiss, fuchsite-bearing quartzite, banded iron formation, stromatolitic marbles and oligomictic meta-conglomerate to sustain the matrix-supported Ediacaran conglomerate of the Barriga Negra Formation (Midot, 1984; Fambrini et al., 2005; Masquelin et al., 2017; Núñez Demarco, 2019). The youngest detrital zircon age peak (n ≥ 3) for the Barriga Negra formation is 581 ± 6 Ma (Blanco et al., 2009; Oyhantçabal et al., 2021).

3. Methods

3.1. Geophysical data processing

Sander Geophysics Limited (SGL, Ottawa) performed and interpreted a partial airborne high-resolution geophysical survey of magnetometry and gamma-ray spectrometry over Uruguay's territory request of the National Directorate of Mining and Geology, Uruguay (DINAMIGE). SGL carried out 196 data acquisition flights. These flights operate between September 2014 and March 2015 (Bates et al., 2016). The airborne survey products were: (i) the magnetic field anomaly map, (ii) the total count radiometric map. The parameters for obtaining the airborne data were as follows: (i) drape of 100 m above the digital altitude surface, (ii) average flight speed: 130 knots (67 m/s), (iii) 400 m flight line spacing, (iv) geomagnetic field parameters used for reduction to the Pole (RTP): inclination varies between −36.4° and −41.8° and declination vary between −7.6° and −15.8°. Radiometric data have enough resolution for lithological recognition. The imaging combines well with the existing geological information (Preciozzi et al., 1985; Bossi et al., 2001). We made an accurate separation of rock units using airborne survey total count radiometric (TCR) data and the horizontal (dx, dy) derivatives of the anomalous magnetic field map reduced to the pole with an upward (1000 m) continuation filter. This filtering accentuates the fields due to different elevations' sources, detecting the main deep-rooted NE-SW and N–S faults. The magnetic and radiometric data aim to re-interpret the entire study area's geological framework (the Nico Pérez Terrane). The total count radiometry combines a shaded relief representation of the 12 m ALOS-Palsar digital elevation model (Advance Land Observing Satellite; UAF-NASA-JAXA, 2011). The software Oasis-Montaj 8.3.0© (Geosoft Inc.) was used to plot geophysical data. Another achievement was the DEM compilation and the total count radiometry map using the software QGis (GNU).

3.2. Analytical dating method

We set up the isotopic data and zircon dating at the Geochronological Laboratory of the Geosciences Institute from the University of São Paulo (Brazil). The LA-ICP-MS equipment locates at the CPGeo-IGc/USP and has an excimer laser of ArF gas (193 nm) coupled to the Neptune™ High-Resolution Multi-collector ICP-MS. The excimer laser used here provides a better regularity of abrasion, reducing the fractionation between masses due to its high optical quality and source stability (Sato et al., 2009). The ICP-MS analytical procedure was calibrated using the international standard zircon Temora-1 standard zircon ($^{206}Pb/^{238}U$ = 0.06683). Results are displayed in $^{206}Pb/^{238}U$ *vs.* $^{207}Pb/^{235}U$ Wetherill's Concordia diagram and $^{206}Pb/^{238}U$ *vs.* $^{207}Pb/^{206}Pb$ Tera-Wasserburg's graph, using IsoplotR (Vermeesch, 2018). Wetherill's Concordia diagrams served both to model magmatic protoliths' concordant age and the systematic radiogenic lead loss due to subsequent geological processes. The zircons were ablated during 40 s in the 193 nm Excimer Laser Ablation System, at 7-6 Hz, 6 mJ and full energy, obtaining spots of ca. 25 μm (Helium: MFC1 = 0.300 L/min, MFC2 = 0.300 L/min, Argon: Aux. = 0.95 L/min, sample = 0.978 L/min).

4. Results

4.1. Geological interpretation using airborne radiometry

Airborne radiometric maps can help to identify faults and geological contacts. The rationale for combining total-count radiometry (TCR) with topography is to check structures already identified by photointerpretation. The aim is to recognise the nature of the respective rocks on both

sides of the discontinuities, considering field information. The structural evidence provided by the combination of geological maps and airborne geophysical data is multifaceted. An in-depth analysis of all the issues cannot be done first-hand. We first documented the main faults to discuss kinematics. Therefore, we checked structural settings for granites and identified tectonic structures. Finally, we build up an integrated geological and geophysical map and profile, showing the most relevant features (Fig. 12).

4.1.1. Main geological contacts and fault-kinematic analysis

The Nico Pérez Terrane is complex because it encloses disrupted basement inliers that inherit many structures from their Paleoproterozoic tectonic framework. The TCR map delimits two main sets of radiometric values, (i) a high-intensity domain westward of the Cueva del Tigre fault (2) and the Sierra de Sosa Shear Zone (c), and (ii) a low-intensity domain eastward of the said discontinuities (Fig. 3). Depleted radiation areas appear in blue tones, while high radiation areas appear in fuchsia to pinkish-white shades. The Pavas Block has the lowest radiometric values in the centre (<800 cps; blue tones). These shallow values represent an elongated N–S strip about 20–30 km wide. The "blue" area coincides with K-feldspar depleted rocks. Only a few "grey gneisses" (metatonalites), amphibole-bearing granitic gneisses or diorites could have a compatible composition in the field. The "blue" area is limited to the south by a mild yellow space that matched with the exposure of metaconglomerates and quartzites, restricting it from the Polanco carbonate area, in which radiometry values are low again. This carbonate area is cut to the east by a 170° striking fault that controlled the Barriga Negra conglomerates and an exposure of muscovite orthogneisses (high radiometry in both cases). Meanwhile, the Santa Lucia Batholith (SL) shows extremely high radiometry values and sharp contacts.

Main faults display kinematic indicators based on the lithological identification at both sides of the discontinuity. The low-radiometry elongated strip corresponding to grey gneisses and amphibolites is crosscut by the Cueva del Tigre dextral strike-slip fault (2), giving two longitudinal halves that led to interpret dextral shearing. This fault converges northwards to the María Albina fault (7) and the Caçapava shear zone from Brazil, as already stated (Oyhantçabal et al., 2018). The eastern-lateral half of the Pavas Block shows a narrow, stretched, and crenulated belt of quartzites, micaschists and marbles, partly belonging to the Las Tetas Complex. The western half shows an exposition of granitic gneisses, amphibolites and intrusive granitoids. Meanwhile, the northern part of the map constitutes an inverted pull-apart full of low-grade metasediments. The pull-apart is between the sinistral María Albina (7) and the Arbolito (6) faults, already known as the "Isla Patrulla - Yerbal region". In the field, the succession shows fold-interference patterns (Preciozzi et al., 1988a, b).

The TCR map (Fig. 3) highlights the presence of lineaments that are interpreted as conjugate faults striking 035° and 170°, respectively (e.g., faults 1 and 4). The Cueva del Tigre (2) is a straight, brittle fault. It overlaps the Sierra de Sosa ductile shear zone (c). The fault (2) is parallel to the Chamamé Fault (4). A sigmoid fragment separated from the

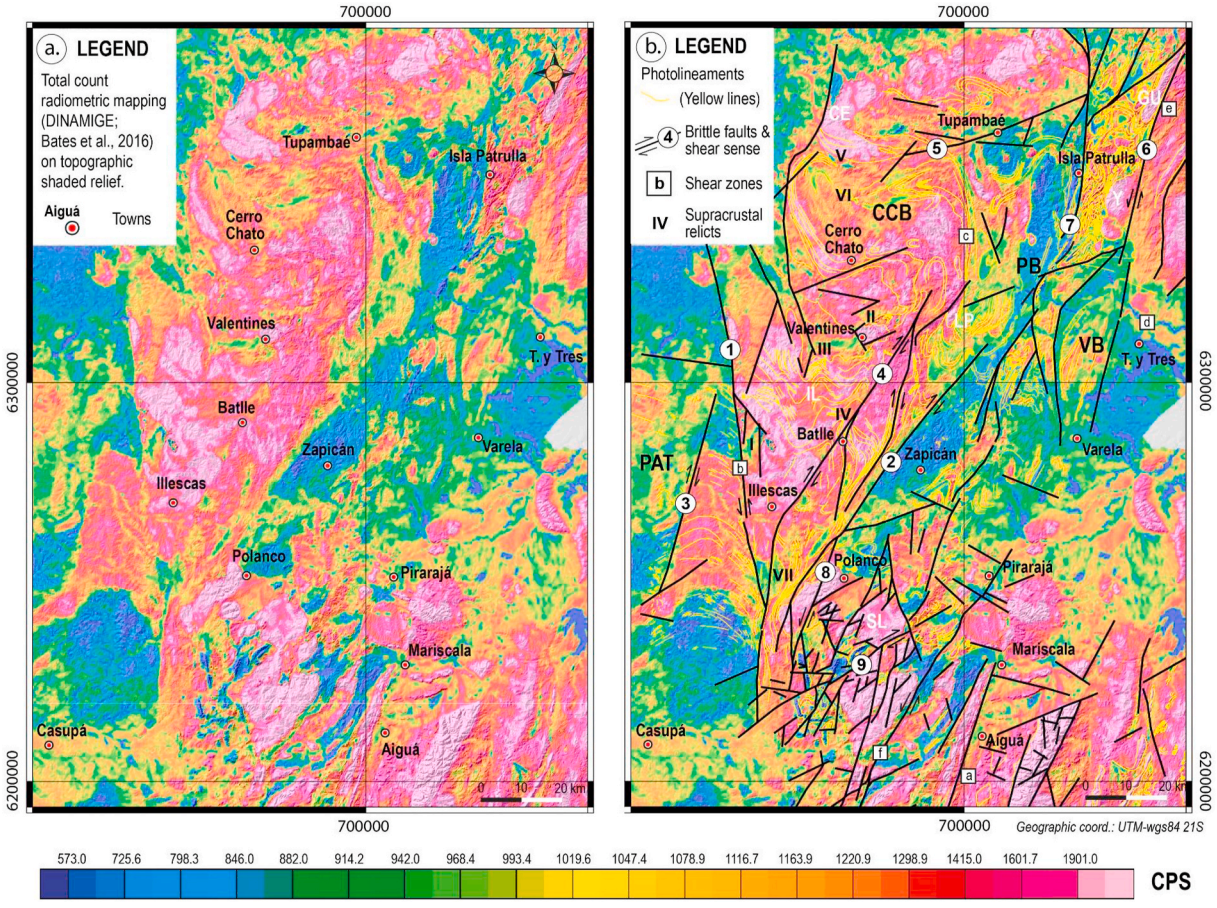

Fig. 3. Airborne total count radiometric map of the Precambrian central domain, combined with the ALOS Palsar topographic shaded relief, presenting the main photo-lineaments (yellow lines) and geological references. Blocks: PAT - Piedra Alta Terrane, CCB - Cerro Chato, PB - Pavas, VSB - Villa Serrana, PET - Punta del Este Terrane; Shear Zones: (a) Sierra Ballena, (b) Sarandí del Yí, (c) Sierra de Sosa, (d) Cerros Amaro, (e) Cerro Largo, (f) Puntas de Pan de Azúcar; *Brittle faults*: (1) Cuchilla Rosario, (2) Cueva del Tigre, (3) Timote, (4) Chamamé, (5) Tupambaé, (6) Arbolito, (7) María Albina, (8) Asperezas, (9) El Soldado; *Supracrustal remnants*: (I) La Pedrera, (II) Valentín, (III) Monzón, (IV) Nico Pérez, (V) Aparicio, (VI) Cañada Rodolfo, (VII) Casupá Chico; Granitoids: SL – Santa Lucia Batholith, LP - Las Palmas Granite, CE - Cerrezuelo Granite, Y - Yerbal Granite, GU - Guazunambí Granite, Y – Yerbal, IL - Illescas.

Illescas granite is among faults 2 and 4 in a strike-slip duplex. The radiometry of this fragment is the same as the leading granite. A dextral shear can be interpreted for the movement of the fault (4). The Illescas Batholith shortened between faults (1) and (4) and is regionally folded. An N–S regional extension (or a general E-W shortening) leads to a north displacement of the Cerro Chato Block, a dextral movement of the Cueva del Tigre fault (2) and a sinistral movement of the Cuchilla del Rosario fault (1). Recognising the lithologies on one side of the fault allows evaluating the dislocation and establishing the shear sense. The Sierra de Sosa Shear Zone is interpreted as a bent lineament, parallel to a sharp lithological boundary with the convexity to the East. It separates layered gneisses and amphibolites, to the East, from alkali-feldspathic granitoids to the West. Although the Pavas Block's northern limit is likely the Tupambaé shear zone (Bates et al., 2016; Oriolo et al., 2016a), the structure seems diffuse and full of granitic intrusions.

The Timote fault (3) strikes 035° and locates within the Piedra Alta Terrane (RPC) (Fig. 3). This fault shows that the RPC margin must have suffered brittle deformation in its interior during the Brasiliano orogenesis since it links to the Sarandí del Yí shear zone. Its conjugate fault is the Cuchilla del Rosario fault (1), which is oriented 170°. The fault (1) appears as a late deformation reactivating the Sarandí del Yí shear zone (b). Cataclastic breccias in dolomites of the Arroyo de la Pedrera Formation (Montaña and Sprechmann, 1993) accounts for the superficial character of this deformation.

4.1.2. Radiometry pattern of supracrustal rocks

In the Cerro Chato Block, there are small, elongated E-W strips, which contrast strongly with the high TCR of surrounding K-feldspar-rich granites (e.g., Illescas granite) (Masquelin, 2006; Loureiro et al., 2019). Their TCR is low (~1000 cps; light green tone) (Fig. 3). Some of them delineate folds or stay at the corner between two conjugate faults. These bands represent erosion remnants of meta-sedimentary sequences, like the Arroyo La Pedrera Formation. We identified at least seven strips of supracrustal rocks that match field observations. This pattern is mainly detected in the Cerro Chato Block.

The 070° dextral Tupambaé fault (5) cuts the contact between the Pablo Paez and the Pavas Block. Oriolo et al. (2016b) already discussed the later generation of this dextral conjugated fault. The radiometry to the north of this Tupambaé fault (5) is equivalent to the Cerro Chato Block. The presence of voluminous Neoproterozoic granites concordant with the gneissic layering (e.g., notably in the Pablo Paez sub-region, e.g., Preciozzi et al., 1979) could explain such elevated radiometry (e.g., Cerrezuelo Granite, CE, dated at ~619 Ma; Fort, 2020), but we cannot confirm that all the concordant granitoids will be Neoproterozoic.

The supracrustal rocks of the Las Tetas Complex only crop out in the Pavas Block. Quartzites and micaschists containing 600 Ma zircons appear in erosive relicts on the Cerro Chato Block. These successions could represent an extensive sedimentary cover deposited (and deformed) at the final stages of the Brasiliano orogenesis. The foliation that affected the different sequences of supracrustal rocks and Paleoproterozoic granitoids appear refolded. The rocks show typical chevron and kink folds. The photo-lineaments (in yellow lines; Fig. 3) represent the foliation directions. Otherwise, the structural interpretation relies mainly on geological maps at the scale of 1:100,000 (Preciozzi et al., 1988a; b, 1989).

In summary, the TCR map shows discontinuous sectors having crenulated foliation with N–S axial-directed folds. The kinks affecting the Las Tetas Complex represent a second tectonic event that overprints this succession. Furthermore, these metasediments were already metamorphic before being affected by this second generation folding. The quartzites have their own radiometric signature (the lowest TCR; deep-blue tone). We can follow this quartzite layer along the eastern border of the La China Complex and south of the Santa Lucia Batholith (SL). However, the Neoproterozoic Yerbal formation cannot be easily separated from the Las Tetas Complex at this scale in the TCR map (Fig. 3).

4.1.3. Geological setting of neoproterozoic granites

Radiometric discrimination of granitoids is possible using different channels (eK, eTh, eU) but is beyond the scope of this work. The shape and relationship with the background allow separating different emplacement settings for granitoids. Using the TCR map, granitoids like the Zapicán diorite, it is challenging to separate them from the La China Complex because both are K-feldspar depleted. However, in most cases, the granite emplacement setting provides a structural classification. Many granitic plutons associate with displacements along the main shear zones. Some already dated plutons related to shear zones help interpret the sense and period of the shearing. The lateral extrusion of Neoproterozoic late-orogenic plutons (e.g., Guazunambí (GU) and Yerbal (Y), i.e., 619 Ma; Fort, 2020) towards the south-west of the sinistral Sierra Ballena Shear Zone (e) is evident (Fig. 3). In the same way, the Las Palmas porphyritic granite (LP) emplaced in the Sierra de Sosa shear zone (c) likely follows a dextral lateral extrusion.

Conversely, the older (633 Ma) and larger Santa Lucia granite (SL) (Bossi et al., 2001) locates in a relatively low-strain location in the south of the Pavas Block. This is a relatively isotropic granite, although slightly broken by brittle faults. Many conjugate 060° and 015° striking faults crosscut the Santa Lucia granite (e.g., faults 8 and 9; Fig. 3). Santa Lucia granite's tectonic blocks overlap through shortening in constriction. The entire body could be an elongated batholith, but now it is just a fragment "transported" by the Pavas Block. Therefore, there is no connection with other granite's fragments in adjacent blocks. Finally, some circumscribed circular post-tectonic granites appear in extensional settings (i.e., Tapes Chico granite). The U–Pb zircon (SIMS) magmatic crystallisation age of the Tapes Chico Granite is 601 ± 5 Ma (Gaucher et al., 2019). Furthermore, this granite yields an $\varepsilon Hf(t) = -31$ and a TDM model age of 3088 Ma.

4.2. Geological interpretation from the anomalous magnetic (dv1) derivative map

The anomalous magnetic (dx1) first derivative map reduced to the pole (RTP) at 1000 m elevation (Fig. 4) reduced the high frequencies. Therefore, it provides information only about the first-order faults. It also emphasises the existence of sharp boundaries between the different blocks of the NPT.

4.2.1. Main geological limits of the Pavas Block

Regarding magnetism, the anomalous magnetic (dx1) derivative RTP map at 1000 m (Fig. 4) shows minimal values in the Pavas Block, while it presents the highest values in the Cerro Chato Block. This map represents the low frequencies. The low-magnetic pattern of the Pavas Block differs clearly from the contiguous Cerro Chato and Villa Serrana blocks. This negative magnetic anomaly may be due to the presence of altered mafic rocks depleted in magnetite. Low-magnetic susceptibility minerals like quartz and feldspar in excess could be present. The upward continuation filter reducing the high frequencies highlights the contrast of the limits, except in the south, where dykes cause high anomalies by interference. In this map, the Sierra de Sosa shear zone resulted in a first-order magnetic boundary.

4.2.2. Superimposed ferromagnetic dyke swarms

Three WNW-ESE Mesozoic dyke swarms crosscut the mapped area. The southernmost swarm seems to be connected by feeder dykes with the Cretaceous Valle Chico Complex (syenites and microsyenites) (Preciozzi et al., 1985). These intrusive complexes represent geological landmarks here. The basement's structural interpretation is difficult near these dyke swarms, mainly in the southernmost sector of the Pavas Block. These dykes are high ferromagnetic dolerites that cause a wide anomaly, even at low frequency. The elimination of high frequencies is not helpful for dyke discrimination if they are too close. Consequently, the magnetic anomaly caused by many thin dykes will cause interference that can blur the magnetic background.

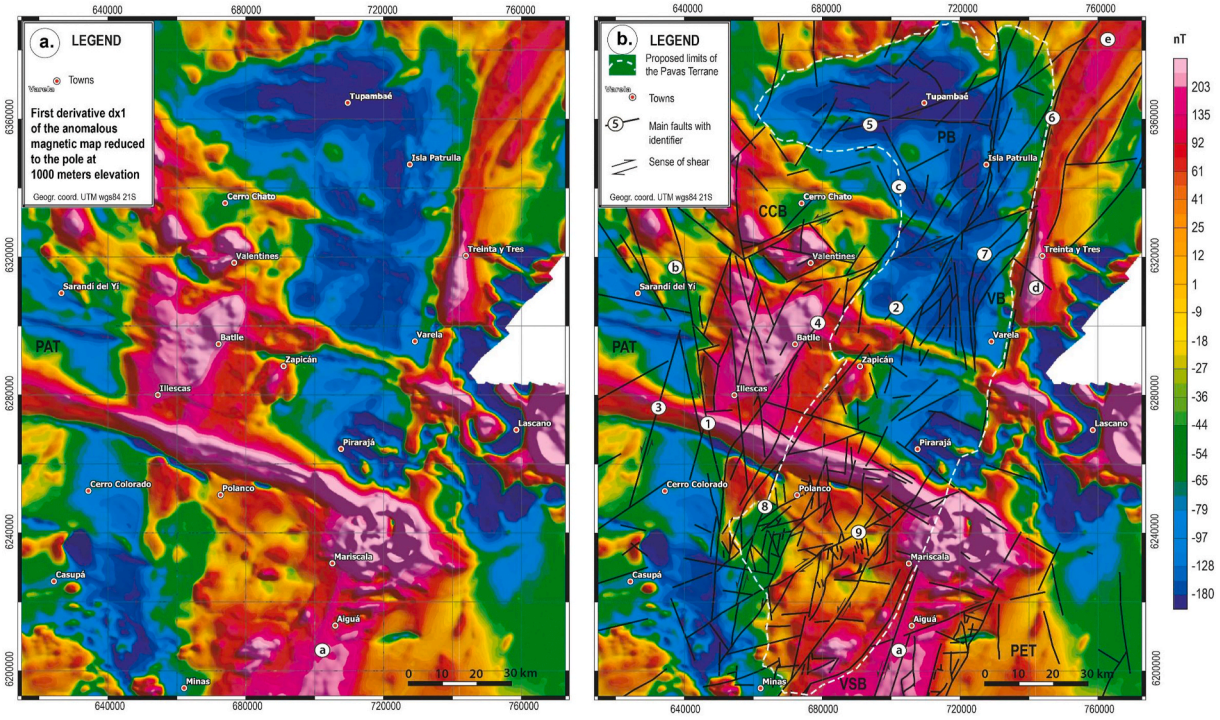

Fig. 4. Airborne magnetic data showing the dx1 horizontal derivative of the reduced to pole (RTP) magnetic anomaly at 1000 m. There is a uniform negative magnetic signature for the Pavas Block except in the southern part due to many mafic dykes (Data from DINAMIGE; Bates et al., 2016). Most of the faults are in the TC radiometric map but highlighted the most magnetic importance (Identifiers are like Fig. 3).

4.2.3. *Main faults and horizontal lateral displacements*

While the Cueva del Tigre Fault (2) is better represented on the TCR map, the Chamamé Fault (4), which is almost parallel to the former one (030°), stands out better on the dx1 anomalous magnetic map. The resulting structure increases the fault visibility with a higher hierarchy and accuracy than those identified by radiometry for the same faults. For example, the Valentines Complex shows rotated square boudins of large dimensions, cut off by 070° and 140° striking faults. These blocks show contrasted high magnetic values (Fig. 3) due to the high magnetic susceptibility of mafic gneisses and BIF found in these blocks. Meanwhile, these boudins appear to be flanked to the south by the Cerro Valentín supracrustal belt (II), which presents weak magnetic susceptibility.

4.3. *Zircon morphology, textures and U–Pb isotope data*

The selected zircons fall within the 70–300 μm grain size fraction. We carried out a comparative aspect ratio. Zircons present different textural features when observed by cathodoluminescence (CL). These microstructures allow us to advance in the knowledge of the metamorphic processes that affected zircons from their origin. In general, there is a significant scattering of the Th/U ratios in almost all the samples (Fig. 5). The bulk zircon histogram shows essentially two main accretion periods in the Archean and the Paleoproterozoic (Fig. 8), although each age interval indicates much more complexity in terms of geological events.

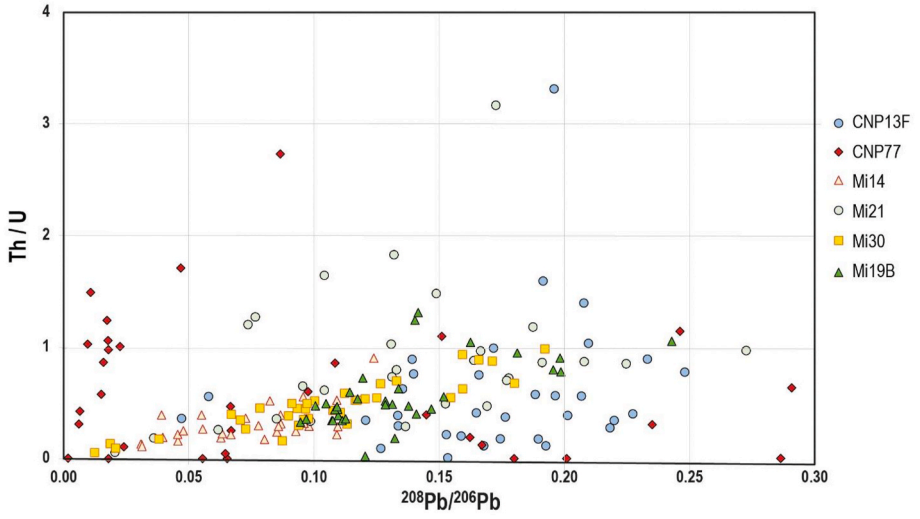

Fig. 5. Th/U vs. $^{208}Pb/^{206}Pb$ correlation diagram for the six zircon samples. Correlation coefficients: CNP13F: +1.000, CNP77: 0.159, Mi21: +0.298, Mi30: +0.585, Mi14: +0.573, Mi19 B: +0.345.

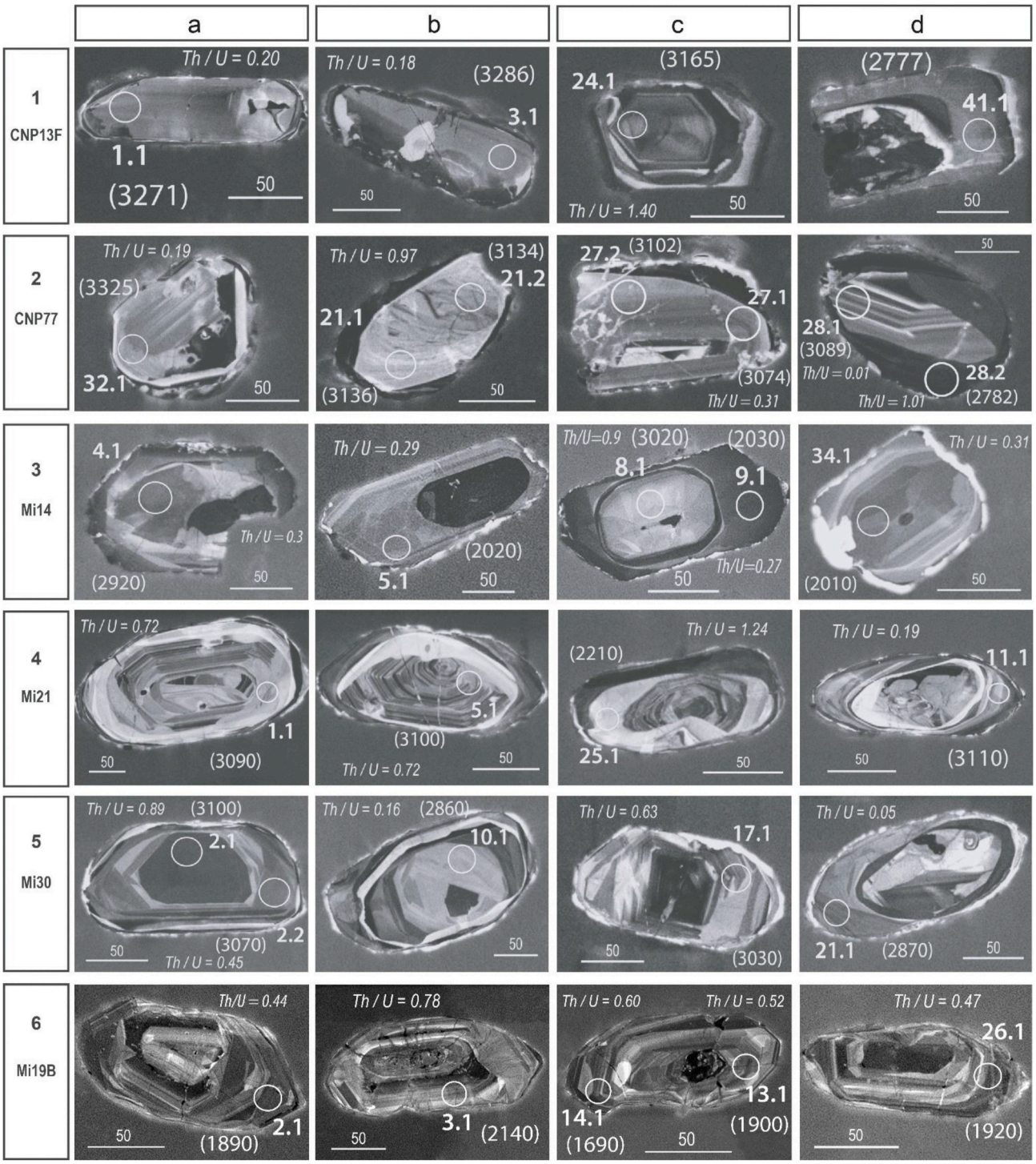

Fig. 6. Textural correlation of zircons between the analysed rocks; each row corresponds to one sample and shows the most prominent zircons in four columns (a, b, c, d) and their textural variations. Circles indicate the LA-ICPMS pit; Th/U values are next to the corresponding spot; scale bar is 50 μm.

4.3.1. Sample CNP13F

This amphibole-bearing gneiss provides an almost regular zircon population (Annexe 1: Fig. 2a–d). Two zircon types are identified, depending on the presence or absence of an inner core (Table II, Annexe 1):

(i) Majority (80%) of misty, pale brown, elongated, subhedral zircons with rounded ends. Their aspect ratio varies from 3:1 to 5:1. Homogeneous, CL-dark zircons have blurred oscillatory zoning pattern (OZP). The overgrowth is practically inexistent. The planar zoning is fading and broadening towards the inner zones. Some features related to transgressive fronts, like void infilling (Figs. 6.1a) or CL-bright internal patches (Figs. 6–1b). Basal prism sections are stubby (aspect ratio 2:1). A secondary recrystallisation patch nucleates in the core-rim interface (Figs. 6.1c). Band replacement shows two transgressive concordant bands, a CL-dark band, and a thin CL-bright trace element-rich seam.

(ii) Few zircons (~10%) show different oval-shaped inherited cores with sharp boundaries, and the overgrowth is vast and unzoned.

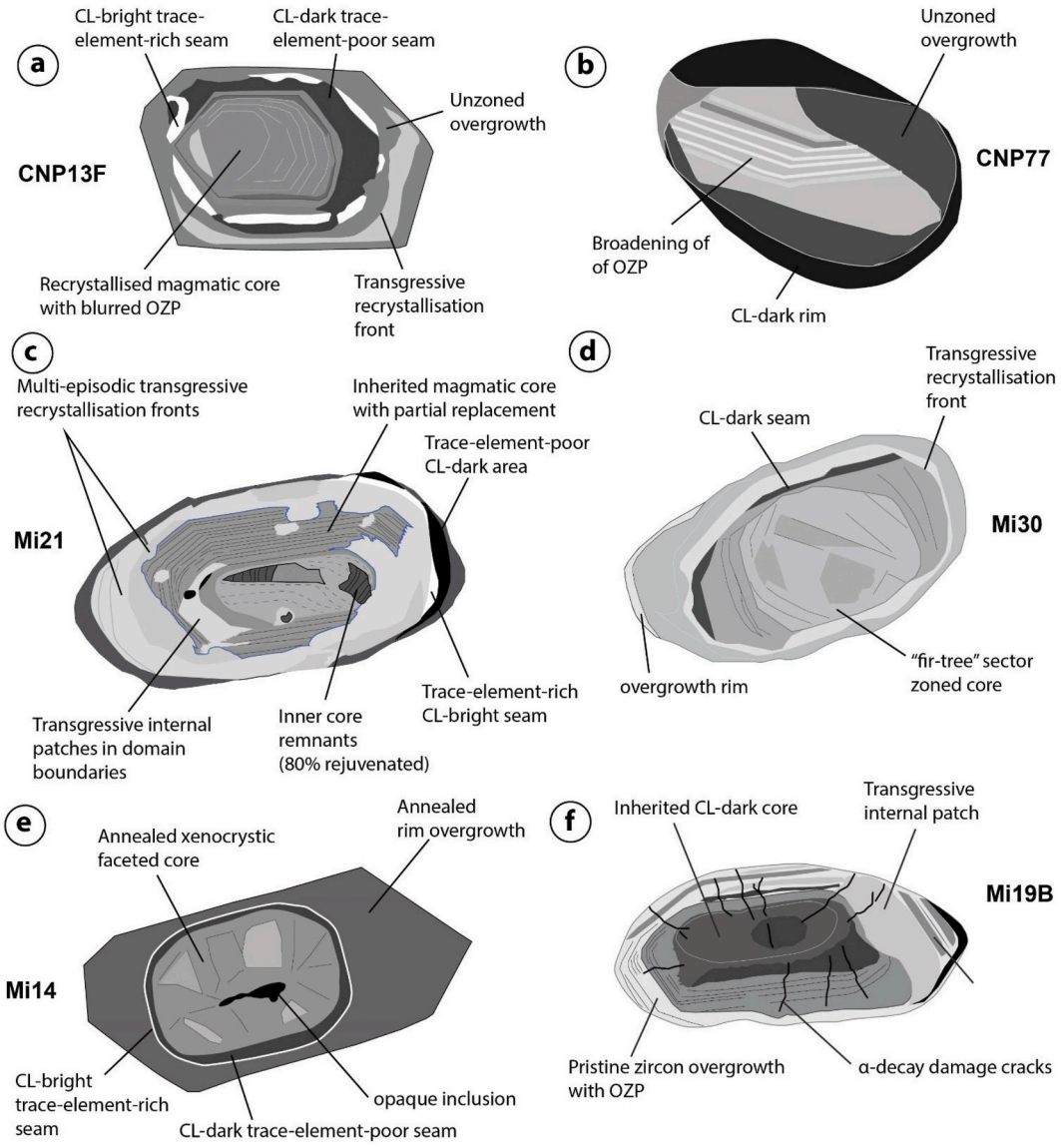

Fig. 7. Selected zircon grains showing the most prominent textural patterns: a) CNP13F-1c; b) CNP77-2 d; c) Mi21-4a; d) Mi30-5 b; e) Mi14-3c; f) Mi19 B-6b.

The core texture is contorted and surrounded by double-coated CL-dark (outer) and CL-bright seams (Figs. 6.1d; Fig. 7a).

There are forty-four useful analyses (Annexe 1: Table I). Only three are in the rims. We plot them in a weighted mean age diagram (Fig. 9a) after filtering data with common lead (Pb*) > 2% and eliminating a few that are further away from the central age bar (Fig. 9b). Therefore, we reduce the MSWD of concordance and increase the probability p(χ^2). However, the method for calculating a central age only reveals that the ages decrease progressively, and there is no valid plateau (Fig. 9b). Then, we apply the "Discordia model-1" (Vermeesch, 2018) after filtering the data (Fig. 9c). We also used a Gaussian and Kernel density diagram (KDE) to discriminate age clusters (Fig. 9c and d). The Discordia line shows an upper intercept at 3270.8±7 Ma and a lower intercept age at ca. 1226 ± 251 Ma (n = 24) (Fig. 9b). Some zircons are reverse-discordant. We relegate higher precision but managed to unravel inherited multiple magmatic sources (~3.33 and 3.26 Ga; MSWD = 1.7). Finally, we applied the (Gray et al., 2008) "Concordia model age" (Vermeesch, 2018) to 11 selected zircons, with the lowest MSWD of concordance (0.03) and the highest probability p(χ^2) = 0.87 (Fig. 9d). Spots located in unzoned overgrowths are scarce (Figs. 6.1d) but yield lower ages (~2.8–3.0 Ga; Fig. 9b). The KDE plot (Fig. 9b) shows multi-stage age clusters at 3.1, 3.25 and ~3.3 Ga (n = 24). Its lower intercept is challenging to interpret without contrasting with other minerals' dating with a lower closing temperature. The concordant age of 3246.8 ± 4.9 Ma (Fig. 9c) resulted from the plot of the same previous data (n = 11), with an MSWD of 0.03 and a probability p(χ^2) = 0.87.

4.3.2. *Sample CNP77*

This sample is extracted from a muscovite orthogneiss emplaced in a flat-lying shear zone (Annexe 1: Fig. 2e–h). There is a mixture of five different zircon types in the sample size (n = 33). All the grains are generally round and stubby. Most zircons show inherited cores and new growth rim. The round grains contain sealed fragments of fractured grains. The zircon types are the following:

(i) Round zircons showing an inner core with OZP (10%), surrounded by an outer body with CL in medium-grey shades and cloudy texture, the whole coated by planar non-luminescent seam and finally by planar CL-bright stitching (Figs. 6.3a).
(ii) Convolute recrystallisation surrounded by tight concordant non-luminescent recrystallisation seams (Figs. 6.3b).
(iii) Fractured zircon containing an inner unzoned core composed of bright and dark CL seams, surrounded by blurred OZP inherited

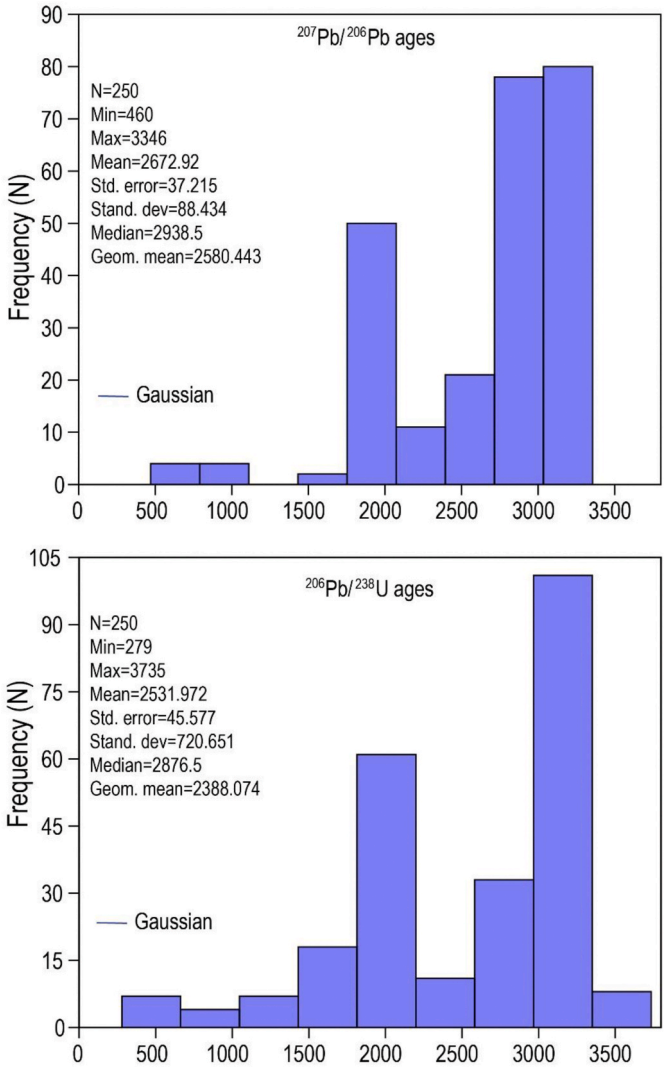

Fig. 8. Bulk $^{207}Pb/^{206}Pb$ (a) and $^{206}Pb/^{238}U$ ages (b) on histogram and statistics for all samples; four maxima for: 1) 3.1–3.2 Ga, 2) 1.9–2.0 Ga, 3) 1.4–1.5 Ga and 4) 0.5–0.6 Ga. One division in the x-axis represents 500 Ma; the y-axis shows the frequency number of zircons.

outer magmatic centres, and fine external overgrowth (bright), and post-recrystallisation fracturing (20%) (Figs. 6.3c).

(iv) Blurred OZP attest to the magmatic inherited origin. A transgressive recrystallisation seam surrounds this sector zoning (Figs. 6.3d) (10%).

(v) Fractured grains are 35% of the sample; high luminescent material filled up the fractures. It witnesses metamict material loss.

There are 36 analysed spots, but the calculations of age only considered 13 spots. Three upper intercept $^{238}U/^{206}Pb$ ages have been determined: (i) 3353 ± 8.8 Ma (MSWD of concordance = 2.0) (n = 4), (ii) 3129 ± 9.0 Ma (MSWD of concordance = 0.01) (n = 4), and (iii) 2976 ± 9.0 Ma (MSWD of concordance = 0.43) (n = 5) (Fig. 9d; Annexe 1: Table I). These multiple ages probably reflect the mixing of zircons in provenance from different Archean rocks. These concordances discriminate: (i) a Paleoarchean (~3.3 Ga) magmatic protolith (Figs. 6.3a), (ii) a Mesoarchean (~3.1 Ga) population (Figs. 6.3d), and (iii) a Neoarchean (~2.8–2.7 Ga) post-peak zircon growth (Figs. 6.3d). The MSWD of concordance is far from 1 except for the oldest group (above 3.3 Ga). However, there are too few samples to be able to conclude. The kernel density plot (KDE) and histogram (n = 27) show a tendency towards the separation of these three groups (Fig. 9d).

4.3.3. Sample Mi21

This Hbl-bearing tonalitic orthogneiss (Annexe 1: Fig. 3a–f) gives subhedral to round and mostly fractured zircons. Their aspect ratio shows a normal distribution (maximum at 2:1). The texture shows a separation between the OZP of the inherited grain and multiple recrystallisation fronts. Fronts go from outside to overlap themselves inside and partially. The overgrowth leads to sector zoning (planar, radial, fir-tree zoning). There are two zircon kinds:

(i) Containing outer (2) and inner (1) cores; OZP is widespread, and secondary recrystallisation obliterated both the rims and bodies (90% of zircons). OZP are relicts of inherited magmatic zircon. Older and darker CL inner cores (1) contain visible OZP (Figs. 6.4a). Both centres (1 and 2) are affected by transgressive recrystallisation fronts. The main OZP's preservation (Core 2) depends on the advance of multiple recrystallisation fronts (Fig. 7c), except for some fading/broadening of specific bands (Figs. 6.4b). An external transgressive front is close to the boundary of core 2 (Figs. 6.4c).

(ii) Complex inner cores (10%) with patchy zoning or convolute pattern, surrounded by bright CL rim (local recrystallisation). CL-dark bands come from secondary dissolution/reprecipitation (Figs. 6.4d; Fig. 7c).

The Mi21 sample provides 36 single spot analyses. Eight zircons come from recrystallisation rims. Typical from these Archean zircons, Th/U values are extremely dispersed (Fig. 5). Two spots yielded a common Pb in excess (>5%), but we assume that many values indicating zero are abnormally low. After making a wide selection of zircons according to the content of common Pb, we determined a concordant age of 3137.5 ± 4.4 Ma (n = 6), with an MSWD of concordance about ca. 0.0052 and a probability $p(\chi^2) = 0.94$ (Fig. 9e). We tried the nominal Pb correction algorithm provided by the IsoplotR program (Vermeesch, 2018) to perform this probability. Then, we conducted another test, applying the Discordia model-1 for overdispersion in the IsoplotR (Fig. 9f). Sixteen spots in these grains define a Pb-loss regression, which intercepts the Concordia at 2986 ± 5 Ma (upper intercept) and 1804 ± 17 Ma (lower intercept) (MSWD = 5). The weighted mean diagram shows the age dispersion corresponding to the lower intercept (MSWD = 22.5) (Fig. 9f).

4.3.4. Sample Mi30

These zircons come from the mesosome of the biotite-bearing migmatitic orthogneiss (Annexe 1: Fig. 4a–f). They are subhedral to round, and the aspect ratio is 2:1. Many of them show fractures and rough borders. Sutured grains provide some cores. They conduct an extreme development of the sector zoning pattern during recrystallisation, but we can interpret the remnants of OZP (Figs. 6.5c). The zircon types are:

(i). Zircons replaced and recrystallised by sector zoning (Figs. 6.5a-b). Planar or angled sector zoning of the type "fir-tree" is typical (Figs. 6.5b; Fig. 7d). This feature affected almost the entire zircon, except CL-bright transgressive fronts crosscutting the rims. The same zoning pattern recrystallises the cores, but CL-darker.

(ii) Zircons with broadened bands issued from OZP (except the CL-dark centre) but surrounded by sector zoning recrystallisation replaces the original bands. Transgressive fronts are conspicuous and achieve the replacement evolution (Figs. 6.5c).

(iii) Zircons enclosing inherited patchy cores, surrounded by CL-dark seam and sector zoning rim (Figs. 6.5d).

The Th/U values follow a perfect regression line (Fig. 5). There are 31 over 36 useful analyses (Annexe 1: Table I); nine are in the rim. One zircon (Mi30–2.1) has two spots in one core (Figs. 6.5a). The grain selection criteria depended on the low common lead contents. The

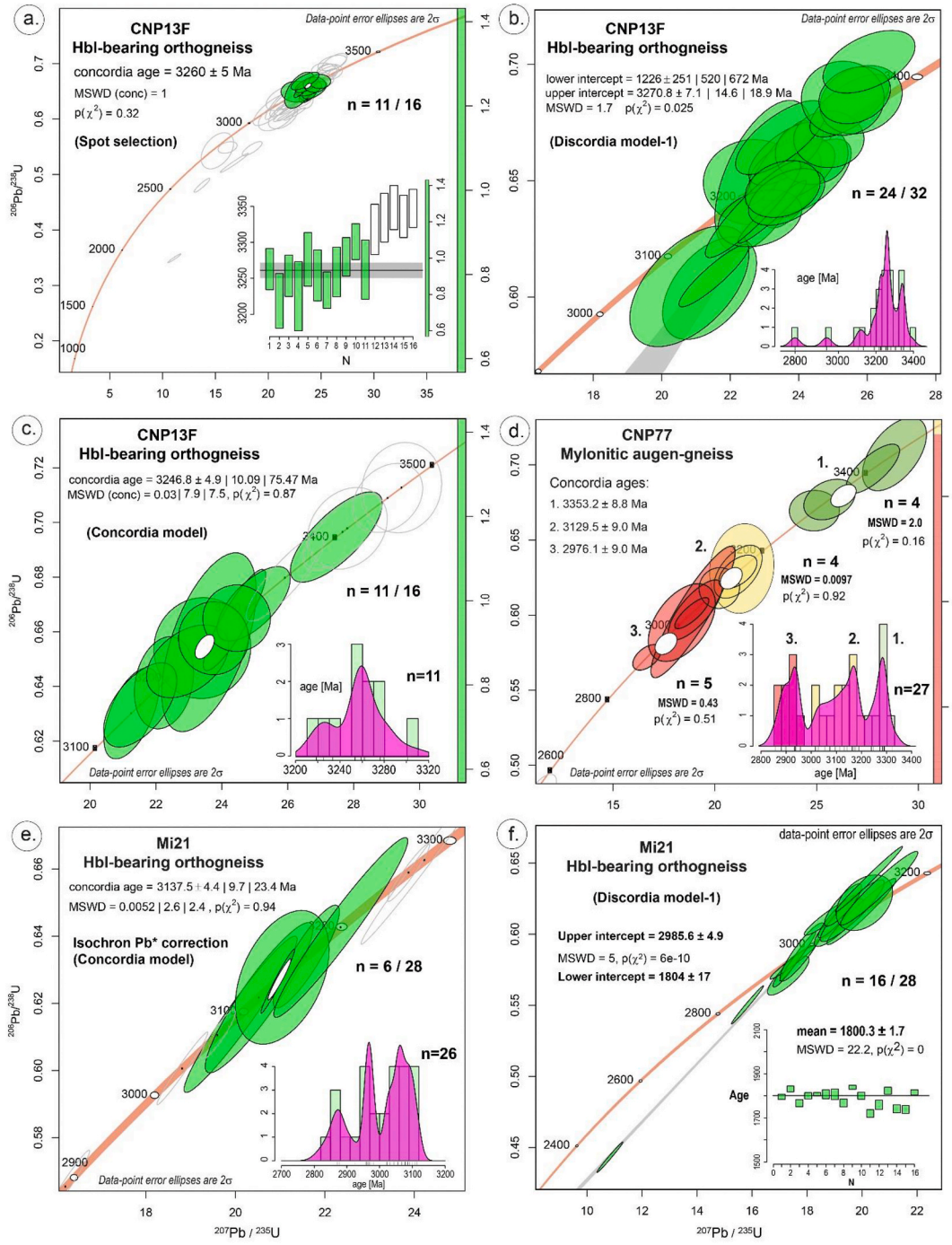

Fig. 9. Concordia plots of U–Pb isotopic analyses of zircon from Archean rocks of La China Complex: (a) Spot selection for Hbl-bearing orthogneiss CNP13F (n = 16) and weighted mean central age diagram suggesting two age groups; (b) Discordia model-1 for the same rock showing a UI age of 3270.8 ± 7 Ma, and a Kernel density estimation (KDE) confirming three age peaks (n = 24); (c) Concordia model for CNP13F zircons showing a protracted distribution with a central age, and the KDE; (d) Concordia ages of the composite augen gneiss and mylonite (CNP77), showing three age groups, and a KDE, confirming these three groups (n = 27); (e) Isochron corrected Concordia age of the Hbl-bearing orthogneiss Mi21 (n = 6) that yields 3137.5 ± 4.4 Ma, and a KDE; (f) Discordia model-1 of the same orthogneiss that yields a UI = 2985.6 ± 4.9 Ma and LI = 1804 ± 17, and the weighted mean age diagram showing 1800.3 ± 1.7 Ma.

Concordia model plot the assignment (n = 10). In this plot, a common lead correction was done according to the Stacey-Kramers function provided by the IsoplotR program (Stacey and Kramers, 1975). We obtained a bimodal data set. The Wederhill diagram shows a concordant age of 3074 ± 7 Ma (MSWD = 1.9) for the oldest data set (Fig. 10a). We performed a second test through the Tera-Wasserburg diagram for the younger data set (n = 31) without common Pb correction (Fig. 10b) that yields a concordant age of 1839.6 ± 2.0 Ma (MSWD = 0.71). A significant over-dispersion of likelihood results displays along with the Concordia (~200 Ma). A Discordia chord shows a connection between both data sets. The younger one is interpreted as the metamorphic replacement/crystallisation age.

4.3.5. *Sample Mi14*

This zircon sample was extracted from a biotite-bearing recrystallised granitoid (Annexe 1: Fig. 5a). The grains are euhedral, fractured,

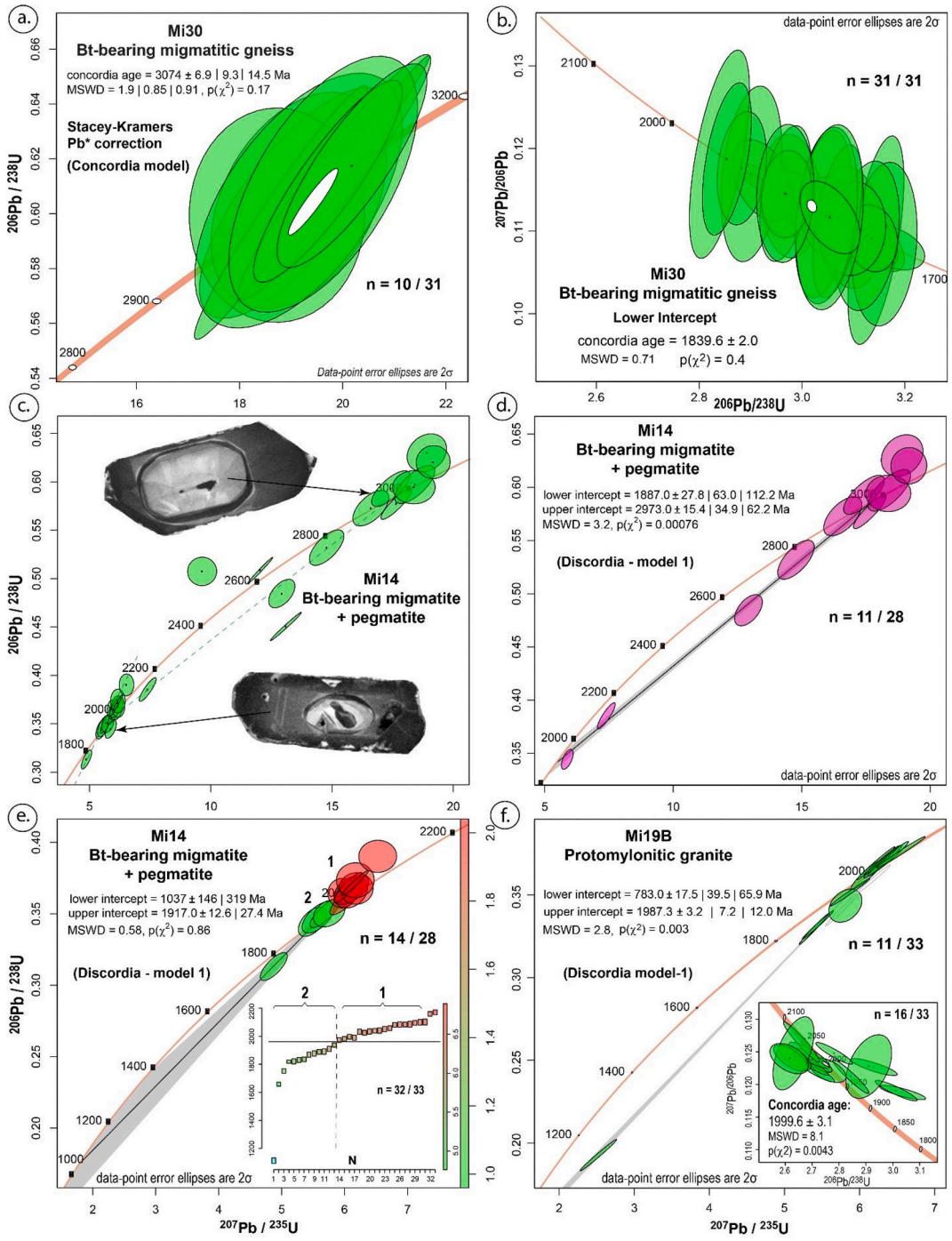

Fig. 10. Concordia plots of U–Pb isotopic analyses of zircon from Rhyacian migmatites and granites of Campanero Unit: (a) Concordia model of the Mi30 Bt-bearing migmatite adding a Stacey-Kramers correction for common Pb (n = 10) that yields 3074 ± 6.9 Ma (inherited age); (b) Concordia model for the same rock in Tera-Wasserburg diagram ($^{207/206}$Pb vs. ^{206}Pb/^{238}U) that yields 1839.6 ± 2 Ma (n = 31); (c) Concordia diagram of the Mi4 migmatite showing the relationship of the zircon part and its corresponding age group; (d) Discordia model-1 for the inherited-zircon age group (n = 11) that yields an UI = 2973 ± 15 Ma and a LI = 1887 ± 28 Ma; (e) Discordia model-1 for the "magmatic and recrystallised" age group (n = 14) in the same sample, yielding an UI = 1917 ± 13 Ma; the weighted mean age diagram below (n = 32) suggest a step among zircons of 2.0 Ga and 1.9 Ga; (f) Discordia model-1 of the mylonitic granite (Mi19 b) that yields an UI = 1987.3 ± 3.2 Ma (n = 11), and below the Concordia model yielding 1999.6 ± 3.1 Ma (n = 16) and showing the disturbance of magmatic zircons.

roughly, and their aspect ratio is 2:1 on average. Many zircons show annealing (core and rim). The annealing produced a multifaceted mosaic texture. Most zircons have an extensive, unzoned overgrowth but generally preserve few oscillatory zoning traces. Annealed zircons have a smooth separation between core and rim, which is interpreted as a chemical recrystallisation front. The annealed cores preserved some relic non-luminescent inclusions. Besides, some patches grew along with different interfaces of zoning. Zircon kinds are the following:

(i) Dark-CL cores with non-luminescent inner parts, enriched in trace elements, seems a relic of the recoil after the annealing. They probably contain porous metamict material (Figs. 6.3a-b) or remnants that were almost wholly solved (Figs. 6.3c-d). The

annealing affected the lattice of many cores (multifaceted appearance). The rim is bright-CL.

(ii) Bright-CL cores, depleted in trace elements, also retain some relic of the recoil after the annealing (Figs. 6.3c). The annealing preserves the euhedral crystal, which could be evidence of magmatic protolith (Fig. 7e). The polygonal aspect of the core; conversely, the rim is dark-CL.

(iii) Pristine zircons without cores. Some centres are CL-dark but small and fuzzy. Some sector zoned broadened bands replaced the original OZP in the body (Figs. 6.3d). There is also some CL-bright transgressive front in the periphery.

We retrieve 36 useful analyses. Th/U show wide dispersed values and total Pb content (%) is high. The plot shows two different populations (Fig. 10c). They correspond to (i) Archean and (ii) Paleoproterozoic zircons. The selected zircons include inherited Archean cores, filtered by low common Pb. We plot two isochrons (IsoplotR - Discordia model-1) (Fig. 10d). The upper intercept yields an age of 2973 ± 15 Ma and the lower intercept age of 1887 ± 28 Ma (MSWD = 3.2). The first is interpreted as the inherited metamorphic/magmatic age of the protolith, whereas the second is considered as the crystallisation age of the new melt. A secondary Pb-loss Discordia regression line yields 1917 ± 12.6 Ma (upper intercept) and 1037 ± 146 Ma (lower intercept) ages (MSWD = 0.58) that is interpreted as Pb-loss resetting due to a second tectonic event. The latter lower intercept is not well constrained (Fig. 10e). A weighted mean age plot shows a drop at ~1.8 Ga.

4.3.6. Sample Mi19 B

This sample comes from a mylonite (K-feldspar granite) sharing the layering with a biotite/tourmaline mica-schist (Annexe 1: Fig. 5b–d). Zircons are dominantly subhedral, multifaceted with a variable aspect ratio (2:1 to 3:1). Also, rounded oval-shaped zircons are present. They are translucent and show weakly-defined oscillatory zoning. Most cores are sector zoned and CL-bright, but the recrystallised oscillatory bands in the centre are broadening (Figs. 6.6a). Radiation damage produced radial cracks, which usually cut the rim overgrowth (Figs. 6.6b; Fig. 7f). Some zircons contain CL-dark, round inner cores. The rims show relics of oscillatory zoning (Figs. 6.6c, d). Transgressive recrystallisation fronts bulge towards the centre. Unzoned patches also appear between the centre and rim (Fig. 7f). The inner core often shows non-luminescent bands surrounded by CL-bright seams. Non-luminescent material locates along with fractures.

Th/U is comparatively less dispersed than in other samples and close to magmatic values (Fig. 5). The zircons of this Paleoproterozoic granite do not have any previous inheritance (e.g., Archean). This sample's Eleven spots gave a poorly constrained Pb-loss regression line (Discordia Model-1) showing highly discordant grains. The isochrone cuts the Concordia at 1987 ± 3 Ma (upper intercept) and at 783 ± 18 Ma (lower intercept) (MSWD = 2.8) (Fig. 10f). An attached Tera-Wasserburg plot using the Concordia model without any corrections shows the natural dispersion of data (n = 16) in the upper intercept giving an age value of 1999.6 ± 3.1 Ma (Fig. 10f). Significantly few 2SE ellipses fall on the Concordia, and the MSWD is higher (8.1). The older age is interpreted as the magmatic crystallisation age. The lower age at 783 ± 18 Ma could be an isotopic disturbance during Neoproterozoic recycling.

5. Discussion

5.1. Interpretation of U–Pb zircon ages and textures

5.1.1. Advances and limitations in the interpretation of U–Pb ages

The relative excess of Pb in most zircons of the La China Complex can be attributed to Pb gain rather than to U and Th loss. Meanwhile, changes in the Pb/U ratio and Pb isotopic composition correlated directly with Pb concentration (e.g., Williams et al., 1984). Pb-gain seems to be a common situation in Archean granitoids. The youngest ~2.7–2.8 Ga zircon ages analysed by SHRIMP in the La China Complex ("sample-1"; Annexe 1: Table III) were considered as formed during a metamorphic event (Hartmann et al., 2001). Their oldest ~3.4 Ga zircon age was interpreted by these authors as the magmatic crystallisation age. However, the reliance between $^{238}U/^{206}Pb$ and $^{207}Pb/^{206}Pb$ is between 102% and 107% in many analysed grains. When applying the Discordia model-2 (Vermeesch, 2018), zircons distribute along with a Pb-loss isochron. The isochron has an upper intercept at 3380 ± 27 Ma and a lower intercept at 2422 ± 100 Ma (n = 12). Our zircon samples CNP13F and CNP77 (Fig. 9a–d; Annexe 1: Table I) come from the same unit a few kilometres from "sample-1". The elevated common Pb makes the concordant age complicated. Archean zircons from igneous protolith likely preserved multi-stage magmatic ages almost unmodified even after being affected by replacement or overgrowth. Zircon textures in the sample CNP13F are typical of high-grade metamorphic rocks (Hoskin and Black, 2000). They consist of a homogeneous population of recrystallised zircons. These zircons almost completely lose their regular oscillatory pattern (Pidgeon et al., 1998; Vavra et al., 1999; Corfu et al., 2003). The fading and broadening of ancient oscillatory zoning are due to recrystallisation/replacement processes (Pidgeon, 1992; Hoskin and Black, 2000). Some grains indicate solid-state recrystallisation within a sustainable closed system (Figs. 6.1b-d) (Schaltegger et al., 1999; Rubatto, 2017). Secondary recrystallisation fronts drive grain boundary migration and defect diffusion to recover trace element accumulation at high-strain lattice settings (Geisler et al., 2007). Trace element partitioning between depleted vs. enriched sectors also provides compelling evidence for solid-state replacement (Pidgeon, 1992; Hoskin and Schaltegger, 2003). Our recrystallised zircons may represent multiple Archean tectono-thermal events. These zircons still have the problem of their protracted residence in conditions above 600 °C, which probably determines the Pb-loss due to slow diffusion over at least 200 Ma. A protracted residence above 600–650 °C is needed to reach the conditions in which metamict zircon is still recovered (Mezger and Krogstad, 1997). This evolution determines a sequential radiogenic Pb-loss due to slow diffusion over time rather than an excess temperature. The apparent "concordance" in the sample CNP13F may be due to the continuous annealing process above the recovering temperature (Mezger and Krogstad, 1997). Considering zircon textures, we assume that the magmatic age exceeded ~3.1 Ga. The Concordia model yields an age of 3247 ± 5 Ma (MSWD of concordance = 0.03; n = 11) (Fig. 9c). The resulting diagram indicates an over-dispersion (spanned from 3300 to 3100 Ma). The excess in common Pb and scattering of Th/U ratios suggest that the U-contents obliterated slowly but deeply during this recycling. The "nearly concordant age" interpretation must consider the youngest zircons as shown to interpret a new zircon growth (Figs. 6.1d). The low-U contents imply that further Pb-loss by recycling will be progressively less effective through time as the U and Th reservoir would be depleted. These scattered ages likely represent the recrystallisation from protracted and continuous magmatic sources >3.1 Ga (Fig. 11) rather than the result of multiple events.

In summary, the La China Complex contains contrasted hornblende-bearing vs. muscovite-bearing orthogneisses. Their protoliths crystallised up to 3.1 Ga. They were further affected by Neoarchean tectono-thermal events (2.7–2.8 Ga). Samples taken from the block's centre did not record any sign of post-Archean recycling. However, the Ar/Ar method shows cooling ages reporting Neoproterozoic reactivation (Oriolo et al., 2016a, b). Otherwise, Pb-gain in zircons could be related to hydrothermal-metasomatic processes typical from the Archean (e.g., Frei et al., 2002). Our samples CNP13F and CNP77 contain three sets of U–Pb ages but slightly different time intervals scattered between ~3.3 Ga and 2.6 Ga (Fig. 9b, c, d; Fig. 11). Still, the CNP77 muscovite gneiss could represent an injected concordant pegmatite emplaced within the flat-lying foliation of a biotite-bearing gneiss in an overthrust (Annexe 1: Fig. 2e–h).

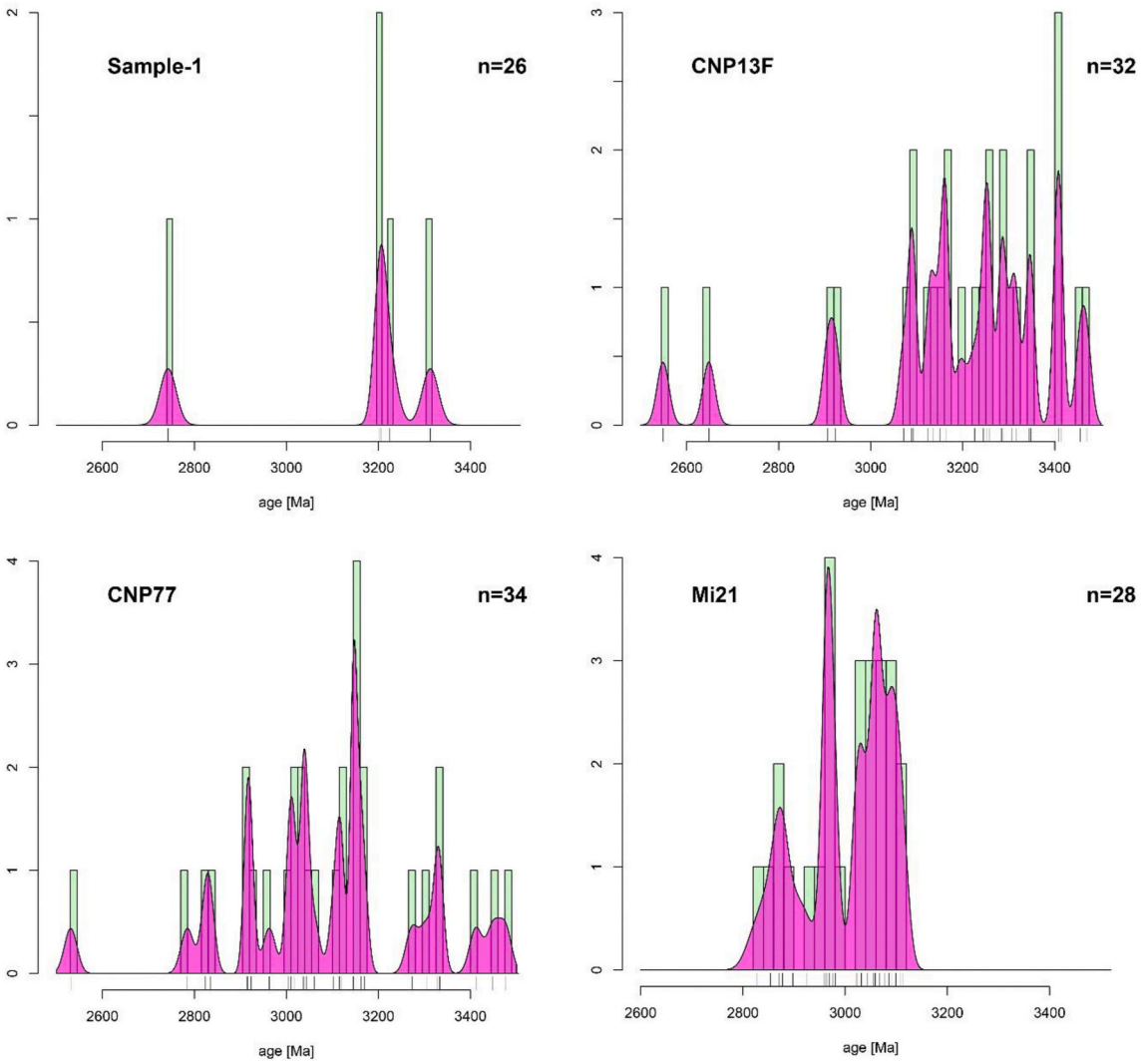

Fig. 11. Correlation of the Kernel Density Estimation about different Archean samples (Sample-1 of Hartmann et al., 2001; CNP13F, CNP77, Mi21, this work).

5.1.2. Episodic magmatic flare-ups during the archean or chaotic inheritance?

A comparative study based on the Kernel density estimation (KDE) between Archean samples (Sample-1; CNP13F; CNP77; Mi21) shows that older clusters are separated by ca. 30–50 Ma, but they are not the same in all the samples (Fig. 11). The bulk U/Pb zircon ages suggest an optimum bandwidth of 25–30 Ma for many key features, which yields approximately 40 peaks with confidence levels of $c \geq 0.9$ (Condie and Aster, 2010). According to Hartmann et al. (2001), Sample-1 shows three peaks: (i) older than 3.30 Ga, (ii) 3.00–3.25 Ga, and (iii) 2.65–2.95 Ga (Fig. 11). CNP13F shows homogeneously recrystallised zircon textures, with blurring magmatic features (Fig. 6.1a–d) and three main age clusters: (i) 3.1–3.4 Ga, (ii) 2.85–2.9 Ga, and (iii) 2.5–2.65 Ga (Fig. 11). However, the concordant data are mostly concentrated up to 3.1 Ga (Fig. 9b, c, d). Meanwhile, these zircons show high dispersion of Th/U ratios and low U contents (<50 ppm) (Annexe 1: Table I). Hartmann et al. (2001) interpreted the rim ages as the M_1 amphibolite facies metamorphism period. La China Complex's samples have in common a scarce record of ca. 2.5–2.9 Ga metamorphic events, but further statistics will require to improve accuracy. The traditionally made inference that zircon U–Pb ages date the intrusion or emplacement of magmatic rocks is difficult to sustain here (e.g., Schaltegger and Davies, 2017). The statistically dominant U–Pb zircon age clusters may reflect the age of source rocks rather than the igneous crystallisation age (e.g., Crowley et al., 2002). Indeed, in such protracted residence (3.4–3.1 Ga), source rocks mainly represent preceding TTG granitoids, which represent ~50% recycled primitive oceanic upper plate, including recycled sedimentary rocks (Frei et al., 2002; Ducea et al., 2015). On the other hand, the magmatic crystallisation interpretation does not forget discriminating between the different multi-episodic pulses of magma accretion separated by lull periods (Ducea et al., 2015). If Archean magmatic arcs were formed in the same way as Phanerozoic's, therefore, Archean magma accretion also characterises as punctuated equilibrium, whereby long periods of quiescence are interrupted periodically by short events of high-volume magmatism called "flare-ups" (DeCelles et al., 2009). This pulsatile behaviour impacts deeply the statistics about the U–Pb zircon ages. The process also affects that of detrital provenance that depends on the same granite sources (e.g., De Silva et al., 2015). The repetition of "nearly concordant" zircon ages in La China Complex could not be explained just by inheritance. On the other hand, there is no record of a single magmatic event that lasts through 300 Ma during the same orogenic event. Paleo-Archean metamorphosed zircons, which show that sparse distribution of "nearly concordant" ages, deserve to be cautiously discussed. Therefore, different generations of multi-stage magmatic zircons could represent an Archean equivalent of the Phanerozoic magmatic flare-ups during protracted subduction (Ducea et al., 2015).

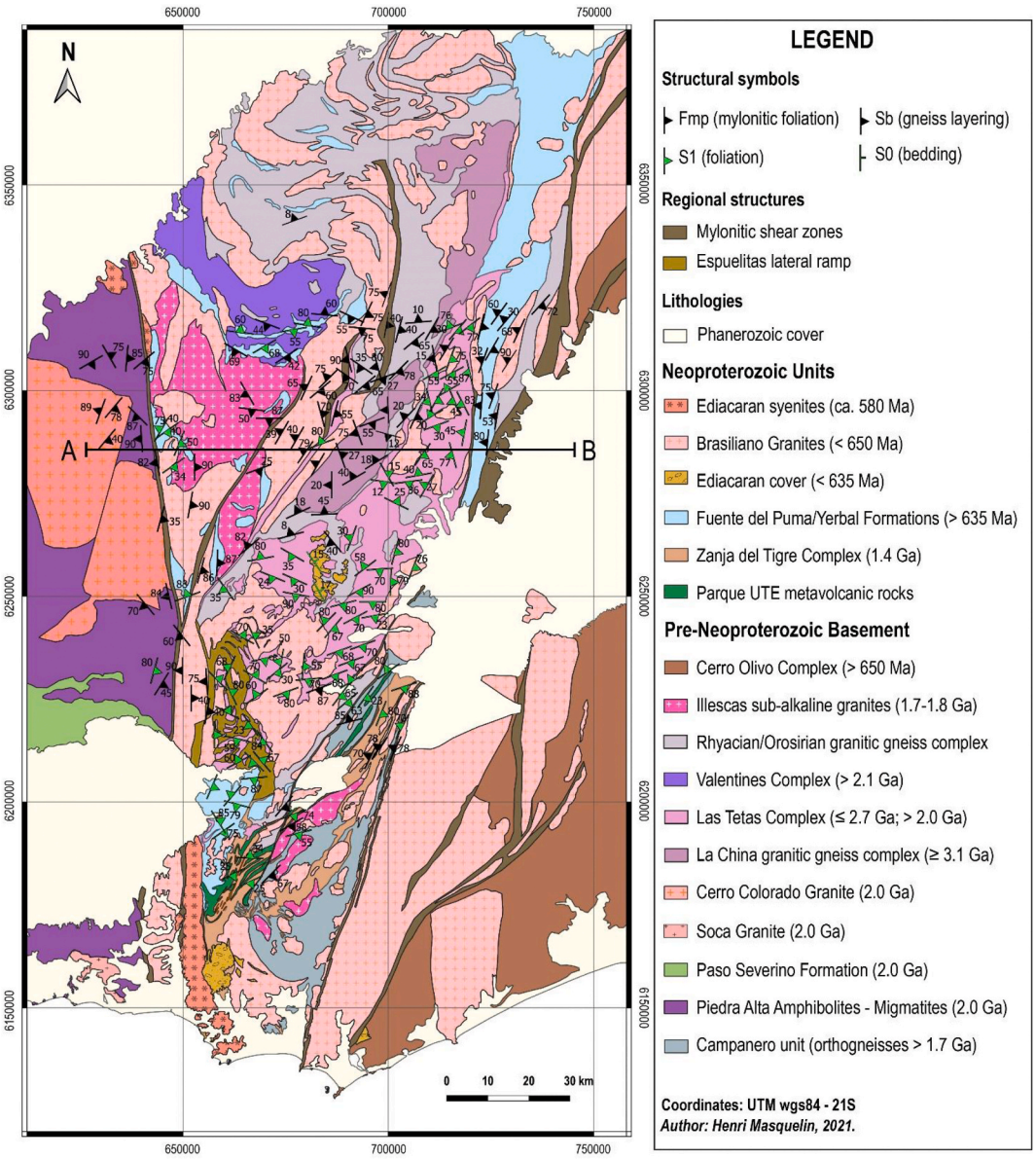

Fig. 12. Geological and geophysical map integration showing the Nico Pérez Terrane and the Pavas Block's most relevant features. Structural-symbols' numbers correspond to the dips. The A-B profiles corresponds to Fig. 13.

5.1.3. What information does the U–Pb system offer about the thrusting age?

The presence of an overthrust carrying muscovite orthogneisses in the middle of the La China Complex, being part of the Sierra de Sosa Transcurrent System (Campal and Schipilov, 1999), was first dated by the K/Ar method, which yields an age of ca. 1253 ± 32 Ma, reported for "synkinematic muscovite" (Bossi et al., 2001). Then, the sample ZAP20 (Gaucher et al., 2011; Annexe 1: Table III) yield a discordant upper intercept age of 3096 ± 45 Ma and a lower intercept of 1252 ± 900 (MSWD = 5.4) (n = 4/12), which conveniently match the K/Ar result. The upper intercept age (~3.1 Ga) was interpreted as the main metamorphic event, but 90% of analyses are in the cores. Our sample CNP77 comes from the overthrust itself. Most of their zircons are rounded and fractured. They are often composed of core and mantle, sector zoning and transgressive recrystallisation fronts (Fig. 7b). These zircons are usually half of the broken prismatic zircons due to grain size reduction by strain (e.g., Corfu et al., 2003). Few zircons that represent the "M_2 metamorphism" yield ~2.6–2.8 Ga (Fig. 9d; Fig. 11). These cracks did not form by radiation damage but also by deformation (Wayne and Sinha, 1988). Indeed, radiation-damaged parts are weak and more likely to nucleate tectonic fractures (Lee and Tromp, 1995). On the other hand, we found a minor assemblage of grains having nebulous zoning or flowing structure, likely formed at granulite-facies conditions (Pidgeon et al., 2000). These zircons yield ages close to ~3.12–3.16 Ga. Otherwise, the oldest zircons yielded ~3.7 Ga, and the youngest ~964 Ma. This age population matches with the overall Archean inherited zircons. Therefore, flat-lying mylonites in sample CNP77 occurred after the Archean. The presence of a ca. 1.0 Ga zircon suggests that the overthrust could be post-Archean but does not produce any measurable overgrowth.

5.1.4. The Orosirian melting and metamorphic overprint

Except for the Archean core, all the peripheral samples from the La China Complex (i.e., Mi21, Mi30, Mi14, and Mi19 b) underwent advanced recycling with metamorphism and anatexis in the Orosirian Period (ca. 2.0–1.8 Ga). Despite the penetrative distribution of this recycling, zircons rarely recorded Neoproterozoic ages. Unlike the Cerro Chato and Rivera blocks, in which Rhyacian magmatism (ca. 2.1 Ga) and

granulitic metamorphism (ca. 2.08 Ga) are widespread (Tickyj et al., 2004; Oyhantçabal et al., 2012; Girelli et al., 2018), these events are not recorded in the Pavas Block. An age lull characterises the Siderian to Rhyacian period at this setting (Fig. 8). In the Orosirian, the South American Platform evolves in many ways, with important accretionary and collisional orogenic events (Brito Neves, 2011). In the Pavas Block, the recycling record of the Orosirian metamorphic event is uneven depending on the site.

The sample Mi21 is a hornblende-bearing metatonalite with magmatic crystallisation at 2986 ± 5 Ma (Fig. 9f; Annexe 1: Fig. 3a–f). The lower intercept at 1804 ± 17 Ma represents a Pb-loss due to amphibolite facies metamorphism (Fig. 9f). Their zircons (Fig. 6.4a–d) shows the best-preserved inherited magmatic textures from a Neo-Archean intrusive granitoid recrystallised by the ~1.8–1.9 Ga metamorphism (Fig. 9e–f). The oscillatory zoning pattern slightly changed during metamorphism, as indicated by bands' broadening (e.g., Pidgeon, 1992). The successive transgressive fronts also preserved the inherited magmatic textures (Fig. 7c).

The sample Mi30 is a layered migmatite that shows complex-textured zircons (Annexe 1: Fig. 4a–f). In this sample, the inherited oscillatory pattern is rare (Figs. 6.5c). The Orosirian migmatites reveal a higher concentration of 1.8–1.9 Ga concordant zircon ages (e.g., Mi30; Fig. 10a). The Th/U regression line (Fig. 5) suggests that the lower intercept connects with the ~1.8 Ga leucosome as a fractionated crystallisation process. However, sector zoning (e.g., "fir tree"; Fig. 7d) or an absence of zoning mostly overlap inherited zircon core's textures. Secondary recrystallisation fronts can mask the new texture partially (Figs. 6.5c). These zircons display bimodal concordant age clusters, one Neoarchean and the other Orosirian (Fig. 10a and b). The 'concordance' model reveals a higher concentration of Orosirian ages at 1839.6 ± 2 Ma (n = 21/31) when applying the common Pb correction algorithms (Vermeesch, 2018). This age is interpreted as melt crystallisation. Although the host rock is not a granulite, "fir tree" zoning may characterise some zircons that underwent granulite-facies conditions (Vavra et al., 1996; Pidgeon et al., 2000; Corfu et al., 2003). The Archean concordant age data cluster represent its granitic protolith (~3074 ± 7 Ma; n = 10/31) (Fig. 10a). This rock was subsequently affected by an Orosirian tectono-thermal event, producing little or no overgrowth. These ratios grown in the presence of partial melt may approach that of igneous zircon due to the monazite anatectic breakdown (Montel, 1993; Kohn and Kelly, 2018). Monazite can destabilise in the melt to form allanite (Lee and Bastron, 1967). Indeed, the allanite is ubiquitous in the neosome of sample Mi30 (Annexe 1: Fig. 4e).

Another sample (Mi14) represents the grey orthogneisses of the La China Complex (Annexe 1: Fig. 6d–h). In this sample, the high-grade metamorphism seems obliterating by low temperature hydrothermalism. Meanwhile, multi-episodic Pb-loss has been recorded in zircons. Sample Mi14 displays an inherited zircon core population yielding an upper intercept age of 2973 ± 15 Ma and a lower intercept of 1887 ± 28 Ma (Fig. 10d). The lower intercept age represents the overgrowths before the second metamorphic event. Then, a Discordia line can be plotted between the upper intercept at 1917 ± 13 Ma and a lower intercept of 1037 ± 146 Ma (Fig. 10e). However, the real interest of this sample is in its texture. Although there are different zircon textures on it, one texture family shows almost complete annealing of cores and rims (Fig. 6.3b-c). This sample is unlikely to come from a granitoid, as evidenced by the unzoned cores, devoid of the oscillatory pattern (Figs. 6.3b-c; Fig. 7e). The oscillatory pattern also lacks in the rims. The polygonal texture indicates partial to complete annealing on these zircons (Fig. 7e). Structural annealing is a common feature in granulitic zircon (Schaltegger et al., 1999; Corfu et al., 2003). Mechanisms proposed as being responsible for redistribution of Pb are the annealing of radiation damage (e.g., Nasdala et al. 2001), fluid alteration (e.g., Geisler et al., 2002), crystal plastic deformation (e.g., Reddy et al., 2006), and annealing due to crystal lattice strain (e.g., Schaltegger et al., 1999). The annealing process represents a reorganization of the zircon lattice in the solid-state. It involves the reestablishment of Zr–O bonds, disrupted by the recoil of the radiation decay (Schaltegger et al., 1999). The driving force may be the differential lattice strain between low-U and high-U growth zones. Radiation damage's annealing is common in natural zircons. Therefore, the recrystallisation process must be occurred by the conjunction between a crystalline recovery of an old, damaged zircon and the overall thermodynamics of metamorphism (Nasdala et al., 2001). In contrast to recrystallisation/replacement, annealing recovery is not necessarily connected with Pb-loss. Hydrothermal fluids may assist post-metamict annealing but do not necessarily reflect a dissolution - reprecipitation process (Geisler et al., 2003). In the case of sample Mi14, we interpret the intermediate age (1917 ± 13 Ma) as the partial melt crystallisation (Fig. 10e). Meanwhile, the lower intercept age reflects a second Pb-loss due to a second tectono-thermal event of ca. 1.1–1.3 Ga. The fluid-enhanced annealing of the amorphous parts in metamict zircons is well-known from hydrothermal alteration experiments (Geisler et al., 2003). Radiation-damaged recovery is a coupled diffusion-reaction and recrystallisation - controlled process (Geisler et al., 2007). In natural zircon submitted to experimental annealing above 830 °C, the recovery occurs in a two-stage process from amorphous material to form new zircon. This process leads to different microstructures, depending on the initial amount of radiation damage. At higher experimental temperature (above 1320 °C), the assemblage transforms into a polygonal texture of small zircon grains (Ginster et al., 2019). In summary, the Orosirian tectono-thermal event is a high-grade metamorphism with different degrees of partial melting and metamorphic recrystallisation on zircons, sometimes coupled with lattice annealing, in the southern and western parts of the Pavas Block.

5.2. Extension of the Pavas Block

5.2.1. What defines the borders of the Pavas Block?

The extension of the Pavas Block does not match that of the exposed Archean rocks. As Mallmann et al. (2007) already stated, *"only a very restricted set of rocks have Archean crystallisation ages."* These rocks have tonalitic protoliths, crystallised from a mantle source between 3.1 Ga to 3.4 Ga. The Sm–Nd TDM model ages in an amphibolite suggest that recycling could be Paleoproterozoic (Mallmann et al., 2007).

The southern border of the Pavas Block is related to an earlier structure connected with the Sarandí del Yí shear zone. This region preserves a flat-lying shear zone remain of almost 20 km wide and 30 km long in the region called Espuelitas (Fig. 12). Supracrustal rocks are involved as roof-pendants. It could be a fragment of an abandoned NW-SE striking lateral ramp, which cannot equate with the actual Sarandí del Yí Shear Zone. This shear zone clearly records a strike-slip movement as judging by the strong parallelism of lineations and upright folds (Masquelin et al., 2017). The sample Mi19 B was collected within one of those folds of the mylonitic foliation. The K-feldspar granite (mylonite) does not show any Archean heritage (Fig. 10f). It yields an upper intercept age of 2000 ± 3 Ga (MSWD = 8), interpreted as magmatic crystallisation. Zircon grains are translucent, U-rich and metamict (α-decay damage cracks). The K-feldspar granite was mostly deformed during the Neoproterozoic (783 ± 18 Ma) under lower amphibolite facies conditions, together with the host rock, a tourmaline-biotite micaschist (Annexe 1: Fig. 5b–d). Another SE-structure near the southern contact is the Mesoproterozoic schist belt, named the Tapes Complex (Gaucher et al., 2019), which results in a natural frontier between the Villa Serrana and Pavas blocks. In summary, all this evidence suggests that the Pavas Block's southern boundary is flanked by abundant Orosirian magmatism. Also, the Espuelitas flat-lying strike-slip shear zone acts as a transitional basement that dislocated during the Cryogenian.

5.2.2. How far the Las Tetas Complex does extend?

Another question concerning the Pavas Block's limits is how far the exposure of the Las Tetas Complex extends (Hartmann et al., 2001). The

field information indicates that all the block has a "basement-cover" structure like any fold-thrust belt (Fig. 13). This mylonite deformed by late folds affecting the Las Tetas Complex and reactivating the basal unconformities behind the La China Complex. Both units share the same low angle mylonitic foliation, verging towards the south.

The Las Tetas Complex's regional extent is continuous for more than a hundred kilometres from the north until Minas's town in the south (Gaucher et al., 2008). Fuchsite-bearing quartzites and metaconglomerates may reach hundreds of meters in thickness (Hartmann et al., 2001). The thrust-stacking produced muscovite-bearing S granitoids with the foliation parallel to the thrust planes within the La China complex (Hartmann et al., 2001). The deformation events that made the overthrust are in amphibolite facies metamorphism. Later upright folds produced the bending of sub-horizontal thrust planes. Muscovite-bearing S-granites crosscut the Las Tetas Complex. The Parque Salus oligomictic metaconglomerate (Midot, 1984; Masquelin, 2006) can be linked with the Las Tetas Complex and the Campanero and Aguila hills fuchsite-bearing quartzites and BIF. Black quartzites, amphibolites, marbles, BIF, tourmaline-biotite schists, and fuchsite quartzites associated with the Villalba Hill Formation (i.e., Bossi and Gaucher, 2004) also represent an equivalent. Finally, the carbonate-quartzite association in the Polanco region describe an extensive carbonate succession as the basement of the Ediacaran Barriga Negra Formation (Masquelin et al., 2017; Núñez Demarco, 2019). We believe that all these rocks may represent equivalents of the Las Tetas Complex. Fuchsite-bearing quartzites and metaconglomerates associated with BIF likely represent lithotypes from Paleoproterozoic marine sequences submitted to pre-Neoproterozoic hydrothermal alteration. The Siderian global climate change at ~2.45 Ga, known as the "Great Oxidation Event" (GOE; Bekker et al., 2004; Konhauser et al., 2011), maybe the cause of chromium solubility and alteration of the Las Tetas Complex. The marked differences in metamorphic grade between the Las Tetas Complex and the Neoproterozoic cover suggest that chromium dispersal was principally Orosirian and syn-metamorphic. Most of the stromatolite-rich dolostones found in different settings between the centre and the extreme south (near the Minas city) are likely related to the Las Tetas Complex. Erosive unconformities found in this region between the Ediacaran cover above the medium-grade metamorphic Las Tetas Complex (e.g., Masquelin et al., 2017) are not affected by the chromium hydrothermalism.

5.2.3. *Contribution concerning the "exotic" Pavas Block*

The NPT proved to be allochthonous concerning the Río de la Plata Craton (Oriolo et al., 2015; Oyhantçabal et al., 2018). However, primary accretion's period preceding the NPT amalgamation is unknown. On the one hand, different inherited heterogeneities must be analysed, like the presence of a disrupted piece of a Neoproterozoic batholith (i.e., Santa Lucia granite; SL) placed transversely in the south of Pavas Block. This granite does not match with any other of the same age (ca. 630 Ma), from the neighbouring blocks. This "exotic" K-feldspar granite crystallised in a low-strain environment, highlighting the complexity of the Neoproterozoic amalgamation in the NPT. On the other hand, the inherited metamorphic grade and the restrained setting of the Las Tetas Complex compared with those of Neoproterozoic units led to questions about the "suspected" provenance of the Pavas Block. This block could be first a Paleoproterozoic terrane displaced during the Rhyacian accretion within the Columbia Paleo-continent, like many others around the São Francisco Craton (e.g., Ávila et al., 2010; Martins-Ferreira et al., 2020) before becoming "Brasiliano".

One of the most accepted ideas concerning the secondary intracontinental amalgamation is that the Dom Feliciano/Kaoko Belt probably ended with an oblique collision and lateral escape or extrusion (Fernandes et al., 1993; Tommasi et al., 1994; De Toni et al., 2021). The Kalahari Craton collision against the 'Rio de la Plata Craton-NPT' assemblage (Philipp et al., 2016) was likely to occur during the last transpression event (Goscombe et al., 2005; Oyhantçabal et al., 2011). This event produced tectonic constriction and lateral extrusion of the NPT. Therefore, interspersed crustal slices coming from different origins are expected (e.g., Burke and Şengör, 1986).

The structural evidence suggests that post-amalgamation tectonics produced subsequent brittle reactivations, along with conjugate faults, like (1) Cuchilla del Rosario, sinistral, and (2) Cueva del Tigre, dextral (Fig. 3).

The Neoproterozoic ductile deformation produced NE-SW foliations parallel to the Dom Feliciano Belt (DFB) on Pavas Block's eastern side. In contrast, it created the reactivation of older E-W structures in the western region. Therefore, the Pavas and Cerro Chato Blocks seem to be allochthonous since the Santa Lucia Granite (SL) has no equivalent in the Cerro Chato Block (Fig. 12). During the building of the DFB (~600-550 Ma), there was an eastward-increasing deformation of the La China Complex and another foreland basement. Strain-localisation through time gives rise to the Sierra Ballena Shear Zone in its current form. The NPT separated into different lens-shaped blocks as soon as the reactivation of inherited internal heterogeneities progressed. The Villa Serrana and Pavas blocks were the most involved in the Neoproterozoic deformation. This region deformed at relatively low temperature during the Neoproterozoic tectonic evolution. Therefore, high-grade metamorphic rocks are inherited from the pre-orogenic foreland. Since then, the removal of large tectonic blocks adapted to accommodate the space problem generated by the E-W shortening between the RPC and the Kalahari Craton during the Ediacaran. This displacement caused rapid and drastic geometric changes in the Dom Feliciano Belt. An initial high angle orientation probably parallel to the RPC's hypothetical northern edge. The Ediacaran orogenesis deformed all the Mesoproterozoic and Neoproterozoic cover successions, except some detrital sequences far away from the faults (e.g., Barriga Negra Formation). The displacement of crustal blocks during the Neoproterozoic collision resulted in the Cerro Chato Block's insertion with an N–S shortening. However, this shortening could have been replaced by an N–S stretching through inversion tectonics during the last Ediacaran transpressive event. In this

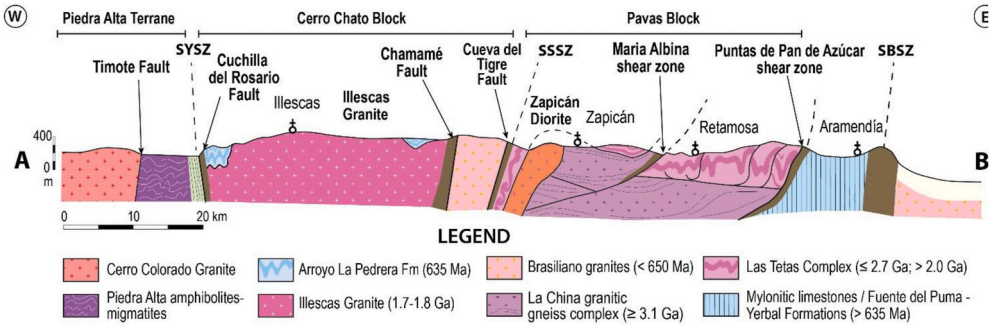

Fig. 13. E-W geological profile cutting the different blocks within the Nico Pérez Terrane, up to the Neoproterozoic schist belt. The over-thrust of the Las Tetas Complex on La China Complex is presented.

new scheme, the Sarandí del Yí shear zone went from dextral to sinistral movement. Meanwhile, its conjugate, the Maria Albina shear zone, went from sinistral to dextral kinematics. The last transpressive event could produce the northwards lateral escape.

5.3. Differences within the adjacent blocks and regional correlations

5.3.1. Geological differences between the NPT blocks

A curved geological contact in the centre of the NPT is coincident with the Sierra de Sosa Shear Zone (Fig. 3). The new map highlights a regional fold affecting the Pablo Paez sub-region (north of the Cerro Chato Block) (Fig. 12). This fold would have developed during the Brasiliano orogenic event (Preciozzi et al., 1979). The Neoproterozoic granites emplaced concordantly within the plastic reactivation of the gneiss layering in the Cerro Chato Block. So far, only the Cerrezuelo granite has been dated at 619 Ma (Fort, 2020), but it emplaced within a hinge in the Cerro Chato Block. The Pablo Paez subregion may be the continuation of the Pavas Block, as shown by the virgation of the Bouguer and magnetic anomalies, despite the proposed disruption along the Tupambaé shear zone from different authors (Bates et al., 2016; Oyhantçabal et al., 2018). The lithologies in the Pablo Paez subregion are orthogneisses and intrusive granites (Preciozzi et al., 1979). Although retrogressed amphibolite facies rocks, there are traces of iron formations, which resemble those of the Valentines Granulite Complex. Guillemain (1911) referred to "walls of hematite-rich ferruginous rock" north of the Tupambaé railway station (Fig. 12). The geology within the Valentines Granulite Complex has another equivalent in the Rivera block. Retrogressed granulitic rocks, including para and orthogneisses, mafic rocks, and ca. 2.1 Ga blue quartz-bearing granites are not present in the Pavas Block. Another difference between the blocks seems to be the lack of Statherian (1.7–1.8 Ga) post-orogenic granitoids in Pavas. Although the Orosirian metamorphism (1.8–1.9 Ga) is common for the while NPT, the Rhyacian granulite metamorphism and magmatism are lack in the Pavas Block. Finally, there are similarities in the zircon detrital ages, as both carry on Rhyacian (2.1–2.2 Ga) and Archean (3.0 Ga) zircon ages to the Neoproterozoic deposits (Oyhantçabal et al., 2021). The strips of shales, carbonate rocks and quartzites that survive erosion on the Cerro Chato block are absent from the Pavas Block, except for some Ediacaran deposits with low strain. Finally, the Neo-Archean/Siderian succession protoliths probably integrate the Valentines granulitic complex. The Villa Serrana Block show traces of BIF and fuchsite-bearing quartzites in roof-pendants of Neoproterozoic granites. The best-preserved Neo-Archean/Siderian succession is still the Las Tetas Complex and it is not present in any other block.

5.3.2. Correlation with other blocks/terranes of the Mantiqueira Province

The Pavas Block can be linked to the "Taquarembó Block" (Hartmann et al., 1999), the Luiz Alves Terrane and the Santa Catarina Granulitic Complex in Southern Brazil (Hartmann et al., 1979; Basei et al., 1992; Siga1995). U–Pb zircon age (SHRIMP) at 2716 ± 0,02 Ga indicates Archean protoliths for the Luiz Alves Terrane (Hartmann et al., 2000). The Luiz Alves Terrane has been subsequently deformed during at least three different metamorphic events. A new investigation shows that U–Pb concordant zircon ages range from 3.2 to 1.8 Ga, indicating a complex evolution (Heller et al., 2021). The titanite crystallised at ca. 2.0 Ga, showing the retrograde path of the Orosirian metamorphism (Camboriú Orogeny). Reverse discordant U–Pb zircon ages indicate that a hydrothermal alteration likely occurred during the Neoproterozoic (Heller et al., 2021). Meanwhile, reverse discordant U–Pb zircon ages from the La China Complex could be due to the same hydrothermalism. The Camboriú Orogeny (2.0–1.8 Ga) affected both the Nico Pérez and Luiz Alves terranes. In Luiz Alves, the oldest inherited zircon age cluster is Mesoarchean (ca. 3.2–3.1 Ga). Other populations yield Neoarchean magmatic ages (ca. 2.7–2.5 Ga). In the Luiz Alves, many zircon grains crystallised during two high-grade metamorphic events at 2352 ± 23 Ma and 2183 ± 17 Ma (Heller et al., 2021). However, the Rhyacian high-grade granulite event of the Rivera-Valentines Complex (2.08 Ga) is younger. Conversely, the Pavas Block does not present any Rhyacian granulitic metamorphism, and ca. 2.5–2.1 Ga old zircons are scarce (see Fig. 8). The Pavas Block shows ~3.0 Ga magmatic crystallisation age from a minor granitoid group (Fig. 9e–f; Fig. 11), younger from the basal La China Complex (≥3.1 Ga). The Pavas Block also includes Hbl-bearing granodiorite (sample SY95; Annexe 1: Fig. 7a–f), which could be Neo-Archean (2.5–2.7 Ga) as well (not yet dated). Other U–Pb zircon data confirmed Neo-Archean granitoids close to the Pavas Block's eastern boundary. Gaucher et al. (2014a) found a magmatic age of ~2.7 Ga near the Sierra Ballena Shear Zone (sample FZ6; Annexe 1: Table III). All these Neoarchean metagranitoids could be correlated to those of (i) the Atuba Complex (Siga et al., 1995; Sato et al., 2003) and (ii) the Camboriú Complex (Basei et al., 2013) (Fig. 1). Most magmatic protoliths in the Atuba Complex point to an age of ~3.0–2.9 Ga that was further affected by the Camboriú orogenic event (~2.0 Ga) (Basei et al., 2013).

Concerning the Las Tetas Complex's correlation, different cratonic successions could match with it in the South American Platform. Lithological associations containing Cr-rich minerals (fuchsite, tourmaline), like the Las Tetas Complex, were reported in the São Francisco Craton (e.g., Barbosa and Sabaté, 2002; Milési et al., 2002; Albert et al., 2018). The Las Tetas Complex may resemble those of the Areião and Contendas-Mirante on the Archean Gavião Block (Barbosa and Sabaté, 2002). The hydrothermal alteration likely occurred in metasediments deposited during the Siderian/Rhyacian interval and succedent metamorphosed like metasedimentary rocks from the Caldeirão Belt (Oliveira et al., 2002). Meanwhile, the protolith succession of Las Tetas Complex has a maximum deposition age of 2764 ± 16 Ma (Hartmann et al., 2001), the detrital provenance of fuchsite quartzites and associated pelitic schists in the Caldeirão Belt is bracketed between 2076 and 2687 Ma by U–Pb SHRIMP in zircon (Oliveira et al., 2002).

6. Conclusion

Geophysical data confirm the separation of the NPT into three blocks. Although brittle faults produced a late orogenic secondary reorganization, the consistency of the Pavas block depends on deeper ductile shear zones. The TCR map and the magnetic anomaly (dx1) confirm the dimensions and limits of the Pavas Block. The magnetic and gravimetric anomalies agree with its dimensions. The TCR map shows high radiometric contrast between the Pavas block and the others. It highlights the abundance of K-feldspar granites in the Cerro Chato Block, while in the Pavas block tonalitic gneisses predominate. Except for the Statherian Illescas granite, the other K-feldspar granites are Neoproterozoic and concordant with the regional gneissic layering. Some elements such as the Santa Lucía granite in the Pavas block are evidence of suspicious allochthony since there is no direct equivalent of this granite in the adjacent blocks. We found the suspicion on the different Paleoproterozoic history of the Pavas Block and the relative absence of Rhyacian and Statherian zircon ages. The southern edges of this block connect with transitional shear zones and the Mesoproterozoic schist belt named the Tapes Complex (Figs. 12 and 13).

The U–Pb zircon dating results indicate a predominance of Archean rocks (~2.7–3.4 Ga), followed by Orosirian magmatic and metamorphic age data (~1.8–2.0 Ga). The La China Complex shows three different zircon clusters: (i) Paleo-Archean (~3.3–3.1 Ga), (ii) Meso-Archean (~3.0–2.9 Ga) and (iii) Neoarchean (~2.7–2.8 Ga). Some zircon rim overgrowths display ~2.7 Ga ages. A reactivated flat-lying mylonite zone in the middle (CNP77) only provides Archean zircons. The thrusting probably occurred during a Paleoproterozoic tectonic event but was thermally reactivated likely during the Mesoproterozoic, which is blind for U–Pb in zircon methods. The southern part of the Pavas Block shows conspicuous Orosirian metamorphism near the contact with the Villa Serrana Block. Zircons yield concordant ~1.8–1.9 Ga U–Pb ages in the overgrowth, interpreted as the partial melt crystallisation, but the

magmatic protolith is Archean. A crustal melting S-type granitoid (e.g., Arroyo Perdido Granite) yields an Orosirian age but extremely negative εHf and Archean TDM model age, confirming the presence of Archean protoliths near the southern end (i.e., Minas town). Archean rocks affected by hydrothermalism are widespread, probably related to the Orosirian metamorphic event. Some gneisses show zircon annealing which can be interpreted as produced by radioactive-damaged recovering assisted by fluids. This process must occur during the retrogressive path and does not involve Pb-loss. An Orosirian K-feldspar granite (~2.0 Ga) without any Archean heritage underwent Neoproterozoic deformation along the flat-lying, strike-slip Espuelitas lateral ramp (Fig. 12). This granite likely set the southern end of the block in a transitional crust. The discovery of a foliated granodiorite crosscutting the La China Complex suggested that later Neoarchean granitoids can be separated from the basal complex. Neoarchean/Siderian metasediments are thrusted on the La China Complex, producing strong N–S stretching lineations parallel to the Dom Feliciano Belt. This succession appears as far as the southern end of the Pavas Block, mostly represented by fuchsite-bearing quartzites/metaconglomerates, carbonates, BIF and amphibolites.

Personal statement

I declare on my honor that this article has been written by me and my co-authors and does not contain any unpublished information unrelated to our research funded by the resources that have been provided by the funding institutions listed in the acknowledgments. Nor do we place a plagiarized copy of any document of another authorship.

Declaration of competing interest

The authors declare that they have no known competing financial interests or personal relationships that could have appeared to influence the work reported in this paper.

Acknowledgements

We thank Bruna Sanches, Nairé Gabriel, and the rest of the team at the Centro de Pesquisas Geocronologicas of the University of São Paulo. We thank Dr Elena Peel for the help regarding the use of standard deviation in the Concordia diagram. We are also indebted to the Director Lic. Nestor Campal, who authorized the use of the airborne geophysical data of DINAMIGE for academic purposes. The authors are grateful to CSIC, UdelaR) for the funding granted (project CSIC-2015 C-604) and to the Faculty of Sciences of the Universidad de la República (Uruguay) for the Logistics. They also acknowledge PEDECIBA - Geosciences who provided grants. To Ecos-sud Conicyt program n°U17U01 for funding the travels and per diem to Tahar Aïfa and Henri Masquelin through a cooperation exchange program between the Rennes 1 and UdelaR universities since 2018. This work is also a contribution to the Unesco-igcp638 program.

References

Albert, C., Lana, C., Gerdes, A., Schannor, M., Narduzzi, F., Queiroga, G., 2018. Archean magmatic-hydrothermal fluid evolution in the Quadrilátero Ferrífero (SE Brazil) documented by B isotopes (LA MC-ICPMS) in tourmaline. Chem. Geol. 481, 95–109.

Almeida, F.F.M., de, Amaral, G., Cordani, U., Kawashita, K., 1973. The Precambrian evolution of the South American cratonic margin south of the Amazon River. In: The South Atlantic. Springer, Boston, MA, pp. 411–446.

Ávila, C.A., Teixeira, W., Cordani, U.G., Moura, C.A.V., Pereira, R.M., 2010. Rhyacian (2.23–2.20 Ga) juvenile accretion in the southern São Francisco craton, Brazil: geochemical and isotopic evidence from the Serrinha magmatic suite, Mineiro belt. J. S. Am. Earth Sci. 29 (2), 464–482.

Babinski, M., Chemale Jr., F., Van Schmus, W.R., Hartmann, L.A., Da Silva, L.C., 1997. U-Pb and Sm-Nd geochronology of the neoproterozoic granitic-gneissic Dom Feliciano belt, southern Brazil. J. S. Am. Earth Sci. 10 (3–4), 263–274.

Barbosa, J.S., Sabaté, P., 2002. Geological features and the Paleoproterozoic collision of four Archean crustal segments of the São Francisco Craton, Bahia, Brazil: a synthesis. An Acad. Bras Ciências 74 (2), 343–359.

Basei, M.A.S., Siga Jr., O., Machiavelli, A., Mancini, F., 1992. Evolução Tectônica dos Terrenos entre os Cinturões Ribeira e Dom Feliciano (PR-SC). Rev. Bras. Geociencias 22 (2), 216–221.

Basei, M.A.S., Siga Jr., O., Masquelin, H., Harara, O.M., Reis Neto, J.M., Preciozzi, F., 2000. The Dom Feliciano belt (Brazil – Uruguay) and its foreland (Rio de la Plata craton): framework, tectonic evolution and correlations with similar terranes of southwestern africa. In: Cordani, Thomaz F° Milani (Ed.), Precambrian Evolution of South America. 31st Int. Geol. Congr., IUGS, Rio de Janeiro, Brazil, 2000, pp. 311–334.

Basei, M.A.S., Frimmel, H.E., Nutman, A.P., Preciozzi, F., Jacob, J., 2005. The connection between the neoproterozoic Dom Feliciano (Brazil/Uruguay) and Gariep (Namibia/South Africa) orogenic belts. Precambrian Res. 139, 139–221.

Basei, M.A.S., Frimmel, H.E., Nutman, A.P., Preciozzi, F., 2008. West Gondwana amalgamation based on detrital zircon ages from Neoproterozoic Ribeira and Dom Feliciano belts of South America and comparison with coeval sequences from SW Africa. Geological Society, London, Special Publications 294 (1), 239–256.

Basei, M.A.S., Campos Neto, M.D.C., Lopes, A.P., Nutman, A.P., Liu, D., Sato, K., 2013. Polycyclic evolution of Camboriú Complex migmatites, Santa Catarina, Southern Brazil: integrated Hf isotopic and U-Pb age zircon evidence of episodic reworking of a Mesoarchean juvenile crust. Braz. J. Genet. 43 (3), 427–443.

Bates, M., McLeish, M., Mushayandebvu, M., 2016. Interpretation Report: Partial Airborne Geophysical Survey of the National Territory and the Procedure and Interpretation of Existing Geophysical Data. Sander Geophysics Ltd., Ottawa, Canada. Contract No. 01/2013, Report for DINAMIGE, 1-654.

Bekker, A., Holland, H.D., Wang, P.L., Rumble, D.I.I., Stein, H.J., Hannah, J.L., et al., 2004. Dating the rise of atmospheric oxygen. Nature 427 (6970), 117–120.

Blanco, G., Rajesh, H.M., Gaucher, C., Germs, G.J., Chemale Jr., F., 2009. Provenance of the Arroyo del Soldado Group (Ediacaran to Cambrian, Uruguay): implications for the paleogeographic evolution of southwestern Gondwana. Precambrian Res. 171 (1–4), 57–73.

Bologna, M.S., Dragone, G.N., Muzio, R., Peel, E., Nuñez-Demarco, P., Ussami, N., 2019. Electrical structure of the lithosphere from Rio de la Plata craton to Paraná basin: amalgamation of cratonic and refertilized lithospheres in SW Gondwanaland. Tectonics 38 (1), 77–94.

Bossi, J., Campal, N., 1991. Granitos negros filonianos del Uruguay: resultados de las investigaciones. In: Proyecto "Granito Negro". Convenio CIID - UdelaR, IDRC - Archivo 90650, p. 72.

Bossi, J., Campal, N., 1992. Magmatismo y tectónica transcurrente durante el Paleozoico inferior en Uruguay. In: Gutiérrez Marco, J.C., Saavedra, J., Rábano, I. (Eds.), Paleozoico inferior de Iberoamérica. Universidad de Extremadura, España, pp. 343–356.

Bossi, J., Gaucher, C., 2004. The Cuchilla dionisio terrane, Uruguay: an allochthonous block Accreted in the cambrian to SW-Gondwana. Gondwana Res. 7 (3), 661–674 doi: 10.1016/S1342-937X (05)71054-6.

Bossi, J., Ferrando, L., Montaña, J., Campal, N., Morales, H., Gancio, F., Schipilov, A., Piñeyro, D., Sprechmann, P., 2001. Memoria explicativa de la Carta Geológica del Uruguay a escala 1:500.000. Fac. Agronomía - UdelaR, pp. 1–122.

Brito Neves, B.B. de, Cordani, U.G., 1991. Tectonic evolution of south-America during the late proterozoic. Precambrian Res. 53 (1–2), 23–40.

Brito Neves, B.B. de, Campos Neto, M.D.C., Fuck, R.A., 1999. From Rodinia to western Gondwana: an approach to the brasiliano-Pan african cycle and orogenic collage. *Episodes*, IUGS 22 (3), 155–166.

Brito Neves, B.B. de, Fuck, R.A., Pimentel, M.M., 2014. The Brasiliano collage in South America: a review. Braz. J. Genet. 44 (3), 493–518.

Bruno, H., Heilbron, M., de Morisson Valeriano, C., Strachan, R., Fowler, M., Bersan, S., et al., 2021. Evidence for a complex accretionary history preceding the amalgamation of Columbia: the rhyacian minas-bahia orogen, southern São Francisco paleocontinent, Brazil. Gondwana Res. 92, 149–171.

Burke, K., Şengör, C., 1986. Tectonic escape in the evolution of the continental crust. In: Reflection Seismology: the Continental Crust, vol. 14. AGU Geodynamics Series, pp. 41–53.

Campal, N., Schipilov, A., 1995. The Illescas bluish-quartz rapakivi granite (Uruguay-South America): some geological features. In: Symposium of Rapakivi Granites and Related Rocks: Belém, Brasil. Abstracts, p. 18.

Campal, N., Schipilov, A., 1999. The eastern edge of the Rio de la Plata Craton: a history of tangential collisions. In: Basement Tectonics, vol. 13. Springer, Dordrecht, pp. 33–48.

Campos Neto, M.C., 2000. Orogenic systems from southwestern Gondwana. An approach to Brasiliano-Pan African cycle and orogenic collage in south-eastern Brazil. In: Cordani, U., Milani, E., Thomaz Filho, A., Campos, D. (Eds.), Tectonic Evolution of South America. Rio Janeiro, pp. 335–365.

Cawood, P.A., Buchan, C., 2007. Linking accretionary orogenesis with supercontinent assembly. Earth Sci. Rev. 82 (3–4), 217–256.

Clark, C., Hand, M., Kelsey, D.E., Goscombe, B., 2007. Linking crustal reworking to terrane accretion. J. Geol. Soc. 164 (5), 937–940.

Condie, K.C., Aster, R.C., 2010. Episodic zircon age spectra of orogenic granitoids: the supercontinent connection and continental growth. Precambrian Res. 180 (3–4), 227–236.

Cordani, U.G., Brito-Neves, B.B., D'Agrella-Filho, M.S., 2003. From Rodinia to Gondwana: a review of the available evidence from South America. Gondwana Res. 6 (2), 275–283.

Corfu, F., Hanchar, J.M., Hoskin, P.W., Kinny, P., 2003. Atlas of zircon textures. Rev. Mineral. Geochem. 53 (1), 469–500.

Crowley, J.L., Myers, J.S., Dunning, G.R., 2002. Timing and nature of multiple 3700–3600 Ma tectonic events in intrusive rocks north of the Isua greenstone belt, southern West Greenland. Geol. Soc. Am. Bull. 114 (10), 1311–1325.
Da Silva, L.C., McNaughton, N.J., Fletcher, I.R., 2005. SHRIMP U–Pb zircon geochronology of Neoproterozoic crustal granitoids (Southern Brazil): a case for discrimination of emplacement and inherited ages. Lithos 82 (3–4), 503–525.
De Silva, S.L., Riggs, N.R., Barth, A.P., 2015. Quickening the pulse: fractal tempos in continental arc magmatism. Elements 11 (2), 113–118.
De Toni, G.B., Bitencourt, M.F., Konopásek, J., Battisti, M.A., da Costa, E.O., Savian, J.F., 2021. Autochthonous origin of the Encruzilhada Block, Dom Feliciano Belt, southern Brazil, based on aero-geophysics, image analysis and PT-paths. J. Geodyn. 144 https://doi.org/10.1016/j.jog.2021.101825, 101825.
DeCelles, P.G., Ducea, M.N., Kapp, P., Zandt, G., 2009. Cyclicity in Cordilleran orogenic systems. Nat. Geosci. 2, 251–257.
Ducea, M.N., Paterson, S.R., DeCelles, P.G., 2015. High-volume magmatic events in subduction systems. Elements 11 (2), 99–104.
Fambrini, G.L., Fragoso-Cesar, A.R.S., de Almeida, R.P., Riccomini, C., 2005. A Formação Barriga Negra (Ediacarano do Uruguai): caracterização estratigráfica e correlação com unidades do estado do Rio Grande do Sul, Brasil. Rev. Bras. Geociencias 35 (4), 515–524.
Fernandes, L.A.D., Tommasi, A., Porcher, C., 1992. Deformation patterns in the southern Brazilian branch of the Dom Feliciano belt: a reappraisal. J. S. Am. Earth Sci. 5 (1), 77–96.
Fernandes, L.A.D., Tommasi, A., Vauchez, A., Porcher, C.C., Menegat, R., Koester, E., 1993. Zona de Cisalhamento Transcorrente Dorsal de Canguçu: caracterização e importância na compartimentação tectônica do Cinturão Dom Feliciano. Rev. Bras. Geociencias 23 (3), 224–233.
Fernandes, L.A.D., Menegat, R., Costa, A.F.U., Koester, E., Porcher, C.C., Tommasi, A., Kramer, G., Ramgrab, G., Camozzato, E., 1995. Evolução tectônica do cinturão Dom Feliciano no escudo sul-rio-grandense: parte I - Uma contribuição a partir do registro geológico. Rev. Bras. Geociencias 25 (4), 351–374.
Fort, S., 2020. Petrografía, geoquímica e isotopía del magmatismo granítico neoproterozoico del Centro-Noreste de Uruguay. PEDECIBA-Geociencias, UdelaR, pp. 1–145. MSc Thesis.
Fragoso Cesar, A.R.S., 1980. O Cráton do Rio de La Plata e o Cinturão Dom Feliciano no Escudo Uruguaio-Sul-Riograndense. In: Congresso Brasileiro de Geologia, 31, Camboriú, 1980. Anais, SBG, vol. 5, pp. 2879–2892.
Frei, R., Rosing, M.T., Waight, T.E., Ulfbeck, D.G., 2002. Hydrothermal-metasomatic and tectono-metamorphic processes in the Isua supracrustal belt (West Greenland): a multi-isotopic investigation of their effects on the Earth's oldest oceanic crustal sequence. Geochem. Cosmochim. Acta 66 (3), 467–486.
Frimmel, H.E., Basei, M.S., Gaucher, C., 2011. Neoproterozoic geodynamic evolution of SW-Gondwana: a southern African perspective. Int. J. Earth Sci. 100 (2), 323–354.
Gaucher, C., Finney, S.C., Poiré, D.G., Valencia, V.A., Grove, M., Blanco, G., Peral, L.G., 2008. Detrital zircon ages of Neoproterozoic sedimentary successions in Uruguay and Argentina: insights into the geological evolution of the Río de la Plata Craton. Precambrian Res. 167 (1–2), 150–170.
Gaucher, C., Frei, R., Chemale, F., Frei, D., Bossi, J., Martínez, G., Chiglino, L., Cernuschi, F., 2011. Mesoproterozoic evolution of the Río de la Plata craton in Uruguay: at the heart of Rodinia? Int. J. Earth Sci. 100 (2–3), 273–288.
Gaucher, C., Bossi, J., Chemale Jr., F., García, G., Frei, R., Frei, D., 2014a. Complejo La China, las rocas más antiguas de Uruguay. In: Bossi, J., Gaucher, C. (Eds.), Geología del Uruguay, vol. 1, pp. 141–154 chp. 5.
Gaucher, C., Frei, R., Sial, A.N., Castiglioni, E., Ferreira, V.P., 2014b. Grupo cebollatí. In: Bossi, J., Gaucher, C. (Eds.), Geología del Uruguay, vol. 1, pp. 155–169 chp. 6.
Gaucher, C., Frei, R., Will, T., Samaniego, L., Ling, X.X., Li, X.H., Li, Q.-L., 2019. Complejo Tapes (Terreno Nico Pérez): edad y relación con otras unidades del Mesoproterozoico de Uruguay. In: 9° Congreso Uruguayo de Geología. Trinidad (4 al 8 Nov): Soc. Urug. Geol., Resúmenes, p. 57.
Geisler, T., Pidgeon, R.T., Van Bronswijk, W., Kurtz, R., 2002. Transport of uranium, thorium, and lead in metamict zircon under low-temperature hydrothermal conditions. Chem. Geol. 191 (1–3), 141–154.
Geisler, T., Pidgeon, R.T., Kurtz, R., Van Bronswijk, W., Schleicher, H., 2003. Experimental hydrothermal alteration of partially metamict zircon. Am. Mineral. 88 (10), 1496–1513.
Geisler, T., Schaltegger, U., Tomaschek, F., 2007. Re-equilibration of zircon in aqueous fluids and melts. Elements 3 (1), 43–50.
Ginster, U., Reiners, P.W., Nasdala, L., Chanmuang, C., 2019. Annealing kinetics of radiation damage in zircon. Geochem. Cosmochim. Acta 249, 225–246.
Girelli, T.J., Chemale Jr., F., Lavina, E.L.C., Laux, J.H., Bongiolo, E.M., Lana, C., 2018. Granulite accretion to Rio de la Plata Craton, based on zircon U-Pb-Hf isotopes: tectonic implications for Columbia Supercontinent reconstruction. Gondwana Res. 56, 105–118.
Goscombe, B., Gray, D.R., 2007. The Coastal Terrane of the Kaoko Belt, Namibia: outboard arc-terrane and tectonic significance. Precambrian Res. 155 (1–2), 139–158.
Goscombe, B., Gray, D., Hand, M., 2005. Extrusion tectonics in the core of a transpressional orogen; the Kaoko Belt, Namibia. J. Petrol. 46 (6), 1203–1241.
Gray R., D., Foster A., D., Meert G., J., Goscombe D., B., Armstrong, R., Trouw J., R.A., Passchier W., C., et al., 2008. A Damara orogen perspective on the assembly of southwestern Gondwana. Geological Society, London, Special Publications 294, 257–278. https://doi.org/10.1144/SP294.14.
Grimes, C.B., Wooden, J.L., Cheadle, M.J., John, B.E., 2015. "Fingerprinting" tectono-magmatic provenance using trace elements in igneous zircon. Contrib. Mineral. Petrol. 170 (5), 1–26.
Guerrero, S., 2016. Geología, petrografía y aspectos macro-, meso-, y microestructurales del área del Salto del Penitente. Trabajo final de Licenciatura en Geología, UdelaR, p. 94.
Guillemain, C., 1911. Zür geologie uruguays. Zeitschr. *Deutsch Geol. Ges.*, Berlin, *Bd.* 63 (4), 203–220.
Harley, S.L., Kelly, N.M., Möller, A., 2007. Zircon behaviour and the thermal histories of mountain chains. Elements 3 (1), 25–30.
Hartmann, L.A., Silva, L.C., Orlandi Filho, V., 1979. O Complexo Granulítico de Santa Catarina. Descrição e implicações genéticas. Acta Geol. Leopoldensia 3 (6), 93–112.
Hartmann, L.A., Leite, J.A.D., McNaughton, N.J., Santos, J.O.S., 1999. Deepest exposed crust of Brazil – SHRIMP establishes three events. Geology 27 (10), 947–950.
Hartmann, L.A., Santos, J.O.S., McNaughton, N.J., Vasconcellos, M.A.Z., Da Silva, L.C., 2000. Ion microprobe (SHRIMP) dates complex granulite from Santa Catarina, Southern Brazil. An Acad. Bras Ciências 72, 559–572.
Hartmann, L.A., Campal, N., Santos, J.O.S., McNaughton, N.J., Schipilov, A., 2001. Archaean crust in the Río de la Plata Craton, Uruguay: SHRIMP U–Pb reconnaissance geochronology. J. S. Am. Earth Sci. 14, 557–570.
Hasui, Y., 1982. The Mantiqueira province: Archean structure and Proterozoic evolution. Rev. Bras. Geociencias 12 (1–3), 167–171.
Heller, B.M., Hueck, M., Passarelli, C.R., Basei, M.A.S., 2021. Zircon U-Pb geochronology and Hf isotopes of the luís Alves terrane: archean to paleoproterozoic evolution and neoproterozoic overprint. J. S. Am. Earth Sci. 106 https://doi.org/10.1016/j.jsames.2020.103008.
Hoskin, P.W.O., Black, L.P., 2000. Metamorphic zircon formation by solid-state recrystallization of protolith igneous zircon. J. Metamorph. Geol. 18 (4), 423–439.
Hoskin, P.W.O., Schaltegger, U., 2003. The composition of zircon and igneous and metamorphic petrogenesis. Rev. Mineral. Geochem. 53 (1), 27–62.
Hueck, M., Oyhantçabal, P., Philipp, R.P., Basei, M.A.S., Siegesmund, S., 2018. The Dom Feliciano belt in southern Brazil and Uruguay. In: Geology of Southwest Gondwana. Springer, Cham, pp. 267–302.
Jost, H., Hartmann, L.A., 1984. Província mantiqueira-setor meridional. In: de Almeida, F.F.M. (Ed.), O Pré-Cambriano Do Brasil. Edgard Blücher Ltd., São Paulo, pp. 345–368.
Kielman, R.B., Nemchin, A.A., Whitehouse, M.J., Pidgeon, R.T., Bellucci, J.J., 2018. U-Pb age distribution recorded in zircons from Archean quartzites in the Mt. Alfred area, Yilgarn Craton, Western Australia. Precambrian Res. 310, 278–290.
Kohn, M.J., Kelly, N.M., 2018. Petrology and geochronology of metamorphic zircon, chapter 2. In: Moser, et al. (Eds.), Microstructural Geochronology: Planetary Records Down to Atom Scale. Geophysical Monograph Series, AGU, pp. 35–61.
Konhauser, K.O., Lalonde, S.V., Planavsky, N.J., Pecoits, E., Lyons, T.W., Mojzsis, S.J., et al., 2011. Aerobic bacterial pyrite oxidation and acid rock drainage during the Great Oxidation Event. Nature 478 (7369), 369–373.
Lara, P., Oyhantçabal, P., Belousova, E., 2020. Two distinct crustal sources for late neoproterozoic granitic magmatism across the Sierra Ballena shear zone, Dom Feliciano belt, Uruguay: whole-rock geochemistry, zircon geochronology and Sr-Nd-Hf isotope evidence. Precambrian Res. 341, 105625.
Lee, D.E., Bastron, H., 1967. Fractionation of rare-earth elements in allanite and monazite as related to the geology of the Mt. Wheeler mine area, Nevada. Geochem. Cosmochim. Acta 31 (3), 339–356.
Lee, J.K., Tromp, J., 1995. Self-induced fracture generation in zircon. J. Geophys. Res.: Solid Earth 100 (B9), 17753–17770.
Loureiro, J., Silva, H., Sánchez Bettucci, L., 2019. Mapa Geológico: el Arqueano en el Uruguay. *Revista Investigaciones*, Montevideo 2 (1), 28-3.
Mallmann, G., Chemale Jr., F., Ávila, J.N., Kawashita, K., Armstrong, R.A., 2007. Isotope geochemistry and geochronology of the Nico Perez terrane, Rio de la Plata craton, Uruguay. Gondwana Res. 12 (4), 489–508.
Martins-Ferreira, M.A.C., Dias, A.N.C., Chemale Jr., F., Campos, J.E.G., Seraine, M., Novais-Rodrigues, E., 2020. Multi-stage crustal accretion by magmatic flare-up and quiescence intervals in the western margin of the São Francisco Craton: U-Pb-Hf and geochemical constraints from the Almas Terrane. Gondwana Res. 85, 32–54.
Masquelin, H., 2006. El escudo uruguayo. In: Veroslavsky, et al. (Eds.), Cuencas Sedimentarias del Uruguay: Paleozoico, vol. 3. DIRAC, UdelaR, pp. 37–106.
Masquelin, H., Silva Lara, H., Sánchez Bettucci, L., Núñez Demarco, P., Pascual, S., Muzio, R., Peel, E., Scaglia, F., 2017. Lithologies, structure and basement-cover relationships in the schist belt of the Dom Feliciano Belt in Uruguay. Braz. J. Genet. 47 (1), 21–42.
Mezger, K., Krogstad, E.J., 1997. Interpretation of discordant U-Pb zircon ages: an evaluation. J. Metamorph. Geol. 15 (1), 127–140.
Midot, D., 1984. Étude géologique et diagnostique métallogenique pour l'exploration du secteur de Minas, Uruguay. Thèse Doctorat 3ème Cycle, Univ. Paris VI, 1 84/24, 1–175.
Milési, J.P., Ledru, P., Marcoux, E., Mougeot, R., Johan, V., Lerouge, C., Skipwith, P., 2002. The Jacobina Paleoproterozoic gold-bearing conglomerates, Bahia, Brazil: a "hydrothermal shear-reservoir" model. Ore Geol. Rev. 19 (1–2), 95–136.
Montaña, J., Sprechmann, P., 1993. Calizas estromatolíticas y oolíticas y definición de la Formación Arroyo de la Pedrera (Vendiano, Uruguay). Rev. Bras. Geociencias 23 (3), 306–312.
Montel, J.M., 1993. A model for monazite/melt equilibrium and application to the generation of granitic magmas. Chem. Geol. 110 (1–3), 127–146.
Murphy, J.B., Nance, R.D., 1991. Supercontinent model for the contrasting character of Late Proterozoic orogenic belts. Geology 19 (5), 469–472.
Nasdala, L., Wenzel, M., Vavra, G., Irmer, G., Wenzel, T., Kober, B., 2001. Metamictization of natural zircon: accumulation versus thermal annealing of radioactivity-induced damage. Contrib. Mineral. Petrol. 141 (2), 125–144.
Neves, Brito, de, B.B., 2011. The Paleoproterozoic in the South American continent: diversity in the geologic time. J. S. Am. Earth Sci. 32 (4), 270–286.

Núñez Demarco, P., 2019. Litodema Tarumán Una secuencia metasedimentaria arqueana del Uruguay. *Revista Investigaciones*, Montevideo 2 (2), 41–53.
Nutman, A.P., Maciejowski, R., Wan, Y., 2014. Protoliths of enigmatic Archaean gneisses established from zircon inclusion studies: a case study of the Caozhuang quartzite, E. Hebei, China. Geoscience Frontiers 5 (4), 445–455.
Oliveira, E.P., Mello, E.F., McNaughton, N., 2002. Reconnaissance U-Pb geochronology of Precambrian quartzites from the Caldeirão belt and their basement, NE São Francisco Craton, Bahia, Brazil: implications for the early evolution of the Paleoproterozoic Itabuna-Salvador-Curaçá orogen. J. S. Am. Earth Sci. 15 (3), 349–362.
Oriolo, S., Oyhantçabal, P., Wemmer, K., Heidelbach, F., Pfänder, J., Basei, M.A., et al., 2015. Shear zone evolution and timing of deformation in the Neoproterozoic transpressional Dom Feliciano Belt, Uruguay. J. Struct. Geol. 92, 59–78.
Oriolo, S., Oyhantçabal, P., Basei, M.A., Wemmer, K., Siegesmund, S., 2016a. The Nico Pérez terrane (Uruguay): from archean crustal growth and connections with the Congo craton to late neoproterozoic accretion to the Río de Rio de la Plata craton. Precambrian Res. 280, 147–160.
Oriolo, S., Oyhantçabal, P., Wemmer, K., Basei, M.A., Benowitz, J., Pfänder, J., et al., 2016b. Timing of deformation in the Sarandí del Yí Shear Zone, Uruguay: implications for the amalgamation of western Gondwana during the Neoproterozoic Brasiliano - Pan - African Orogeny. *Tectonics,* AGU 35 (3), 754–771.
Oriolo, S., Oyhantçabal, P., Konopásek, J., Basei, M.A., Frei, R., Sláma, J., Wemmer, K., Siegesmund, S., 2019. Late paleoproterozoic and mesoproterozoic magmatism of the Nico Pérez terrane (Uruguay): tightening up correlations in southwestern Gondwana. Precambrian Res. 327, 296–313. https://doi.org/10.1016/j.precamres.2019.04.012.
Oyhantçabal, P., Vaz Chaves, N., 1990. Una asociación de cuarcitas y rocas máficas y ultramáficas en los alrededores de Isla Patrulla (Departamento de Treinta y Tres). Resúmenes ampliados del Primer Congreso Uruguayo de Geología. In: Congreso Uruguayo de Geología, I. Montevideo, 25-27 abr. 1990, Actas.
Oyhantçabal, P., Muzio, R., De Souza, S., 1993. Geología y aspectos estructurales del borde orogénico en el extremo sur del cinturón Dom Feliciano. Rev. Bras. Geociencias 23 (3), 296–300.
Oyhantçabal, P., Siegesmund, S., Wemmer, K., Presnyakov, S., Layer, P., 2009. Geochronological constraints on the evolution of the southern Dom Feliciano belt (Uruguay). J. Geol. Soc. 166 (6), 1075–1084.
Oyhantçabal, P., Siegesmund, S., Wemmer, K., Passchier, C.W., 2011. The transpressional connection between Dom Feliciano and Kaoko belts at 580-550 Ma. Int. J. Earth Sci. 100 (2–3), 379–390.
Oyhantçabal, P., Wagner-Eimer, M., Wemmer, K., Schulz, B., Frei, R., Siegesmund, S., 2012. Paleo- and neoproterozoic magmatic and tectonometamorphic evolution of the isla cristalina de Rivera (Nico Pérez terrane, Uruguay). Int. J. Earth Sci. 101 (7), 1745–1762.
Oyhantçabal, P., Oriolo, S., Philipp, R.P., Wemmer, K., Siegesmund, S., 2018. The Nico Pérez terrane of Uruguay and south-eastern Brazil. In: Geology of Southwest Gondwana. Springer, Cham, pp. 161–188.
Oyhantçabal, P., Oriolo, S., Wemmer, K., Basei, M.A.S., Frei, D., Siegesmund, S., 2021. Provenance of metasedimentary rocks of the western Dom Feliciano Belt in Uruguay: insights from U–Pb detrital zircon geochronology, Hf and Nd model ages, and geochemical data. J. S. Am. Earth Sci. 108, 103139.
Pearce, J.A., 2014. Geochemical fingerprinting of the Earth's oldest rocks. Geology 42 (2), 175–176.
Peel, E., Bettucci, L.S., Basei, M.A.S., 2018. Geology and geochronology of Paso del Dragón Complex (north-eastern Uruguay): implications on the evolution of the Dom Feliciano Belt (Western Gondwana). J. S. Am. Earth Sci. 85, 250–262.
Peçoits, E., Aubet, N.R., Heaman, L.M., Philippot, P., Rosière, C.A., Veroslavsky, G., Konhauser, K.O., 2016. U-Pb detrital zircon ages from some Neoproterozoic successions of Uruguay: provenance, stratigraphy, and tectonic evolution. J. S. Am. Earth Sci. 71, 108–130.
Philipp, R.P., Pimentel, M.M., Chemale Jr., F., 2016. Tectonic evolution of the Dom Feliciano belt in southern Brazil: geological relationships and U-Pb geochronology. Braz. J. Genet. 46, 83–104.
Pidgeon, R.T., 1992. Recrystallization of oscillatory zoned zircon: some geochronological and petrological implications. Contrib. Mineral. Petrol. 110 (4), 463–472.
Pidgeon, R.T., Nemchin, A.A., Hitchen, G.J., 1998. Internal structures of zircons from Archaean granites from the Darling Range batholith: implications for zircon stability and the interpretation of zircon U-Pb ages. Contrib. Mineral. Petrol. 132 (3), 288–299.
Pidgeon, R.T., Nemchin, A.A., Kinny, P.D., 2000. Fir-tree and nebulously zoned zircons from granulite-facies rocks: evidence for zircon growth and interaction with metamorphic fluids. Goldschmidt 2000. Int. J. Conf. Abstr. 5, 798.
Preciozzi, F., 1989. Memoria explicativa del fotoplano Zapicán (F-22). In: Carta Geológica del Uruguay. DINAMIGE - UdelaR, Montevideo, p. 12.
Preciozzi, F., Spoturno, J., Heinzen, W., 1979. Carta geo-estructural del Uruguay, escala 1:2.000.000. Instituto Geológico Ing. Terra Arocena, Montevideo, p. 76.
Preciozzi, F., Spoturno, J., Heinzen, W., Rossi, P., 1985. Memoria Explicativa de la Carta Geológica del Uruguay a la escala 1:500.000. DINAMIGE-M.I.E.M. Montevideo, p. 90.
Preciozzi, F., Pena, S., Arrighetti, R., 1988a. Memoria explicativa del fotoplano Isla Patrulla (E-19). DINAMIGE - UdelaR, Montevideo, p. 13.
Preciozzi, F., Pena, S., Arrighetti, R., 1988b. Memoria explicativa del fotoplano Puntas del Yerbal (E-18). DINAMIGE - UdelaR, Montevideo, p. 12.
Rapela, C.W., Fanning, C.M., Casquet, C., Pankhurst, R.J., Spalletti, L., Poiré, D., Baldo, E.G., 2011. The Rio de la Plata craton and the adjoining Pan-African/brasiliano terranes: their origins and incorporation into south-west Gondwana. Gondwana Res. 20 (4), 673–690.
Reddy, S.M., Timms, N.E., Trimby, P., Kinny, P.D., Buchan, C., Blake, K., 2006. Crystal-plastic deformation of zircon: a defect in the assumption of chemical robustness. Geology 34, 257–260.
Roberts, N.M., Spencer, C.J., 2015. The zircon archive of continent formation through time. Geological Society, London, Special Publications 389 (1), 197–225.
Rodríguez, P., Veroslavsky, G., Soto, M., Marmisolle, J., Gristo, P., de Santa Ana, H., Benvenuto, A., 2015. New integrated Bouguer gravity anomaly map onshore Uruguay: preliminary implications for the recognition of crustal domains. In: SEG Technical Program, Expanded Abstracts. Society of Exploration Geophysicists, pp. 1515–1519.
Rosière, C.A., Heimann, A., Oyhantçabal, P., Santos, J.O.S., 2018. The iron formations of the South American platform. In: Geology of Southwest Gondwana. Springer, Cham, pp. 493–526.
Rubatto, D., 2017. Zircon: the metamorphic mineral. Rev. Mineral. Geochem. 83 (1), 261–295.
Sánchez Bettucci, L., Preciozzi, F., Basei, M.A.S., Oyhantçabal, P., Peel, E., Loureiro, J., 2003. Campanero Unit: a probable Paleoproterozoic basement and its correlation to other units of south-eastern Uruguay. In: IV South American Symposium on Isotope Geology, Short Papers, 673-674. CBPM; IRD, Salvador.
Sánchez Bettucci, L., Peel, E., Oyhantçabal, P., 2010. Precambrian geotectonic units of the Río de Rio de la Plata craton. Int. Geol. Rev. 52 (1), 32–50.
Sánchez Bettucci, L., Loureiro, J., Demarco, P.N., 2021. Airborne geophysical characterization of Uruguayan basement. J. S. Am. Earth Sci. 108 https://doi.org/10.1016/j.jsames.2021.103206, 103206.
Santos, J.O., Hartmann, L.A., Bossi, J., Campal, N., Schipilov, A., Piñeyro, D., McNaughton, N.J., 2003. Duration of the trans-amazonian cycle and its correlation within south America based on U-Pb SHRIMP geochronology of the La Plata craton, Uruguay. Int. Geol. Rev. 45 (1), 27–48.
Sato, K., Siga Jr., O., Nutman, A.P., Basei, M.A.S., McReath, I., Kaulfuss, G., 2003. The Atuba complex, southern south American platform: archean components and paleoproterozoic to neoproterozoic tectonothermal events. Gondwana Res. 6 (2), 251–263.
Sato, K., Basei, M.A.S., Siga Júnior, O., Sproesser, W.M., Onoe, A.T., 2009. Excimer laser (193 nm) acoplado ao ICP-MS Neptune: primeiros resultados de análises isotópicas. In: Simpósio 45 Anos de Geocronologia no Brasil. Resumos Expandidos. USP, pp. 131–133.
Schaltegger, U., Davies, J.H., 2017. Petrochronology of zircon and baddeleyite in igneous rocks: reconstructing magmatic processes at high temporal resolution. Rev. Mineral. Geochem. 83 (1), 297–328.
Schaltegger, U., Fanning, C.M., Günther, D., Maurin, J.C., Schulmann, K., Gebauer, D., 1999. Growth, annealing and recrystallization of zircon and preservation of monazite in high-grade metamorphism: conventional and in-situ U-Pb isotope, cathodoluminescence and microchemical evidence. Contrib. Mineral. Petrol. 134 (2–3), 186–201.
Scherer, E.E., Whitehouse, M.J., Munker, C., 2007. Zircon as a monitor of crustal growth. Elements 3 (1), 19–24.
Şengör, A.M.C., Dewey, J.F., 1990. Terranology: vice or virtue? Phil. Trans. Roy. Soc. Lond. Math. Phys. Sci. 331 (1620), 457–477.
Siga Jr., O., Basei, M.S., Neto, J.R., Machiavelli, A., Harara, O.M., 1995. O Complexo Atuba: um cinturão Paleoproterozoico intensamente retrabalhado no Neoproterozóico. *Boletim IG-USP*. Série Científica 26, 69–98.
Silva Lara, H., Masquelin, H., Núñez Demarco, P., 2018. Formación Polanco: petrografía, estructura y metamorfismo en la región de Polanco-Manguera Azul. *Revista Investigaciones.* Montevideo 1 (2), 17–29.
Singh, V.K., Slabunov, A., 2016. Two types of Archaean supracrustal belts in the Bundelkhand Craton, India: geology, geochemistry, age, and implication for craton crustal evolution. J. Geol. Soc. India 88 (5), 539–548.
Stacey, J.T., Kramers, J.D., 1975. Approximation of terrestrial lead isotope evolution by a two-stage model. Earth Planet Sci. Lett. 26 (2), 207–221.
Tickyj, H., Hartmann, L.A., Vasconcellos, M.A.Z., Philipp, R.P., Remus, M.V.D., 2004. Electron microprobe dating of monazite substantiates ages of major geological events in the southern Brazilian shield. J. S. Am. Earth Sci. 16, 699–713.
Tommasi, A., Vauchez, A., Fernandes, L.A., Porcher, C.C., 1994. Magma-assisted strain localization in an orogen-parallel transcurrent shear zone of southern Brazil. Tectonics 13 (2), 421–437.
UAF-NASA-JAXA, 2011. ALOS Palsar RTC, Fine Dual Beam Polarization (FBD) Data Coverage. (2011). PALSAR RT1 DEM, ASF, DAAC [6/5/2015]. [doi: 10.5067/JBYK3J6HFSVF]. https://asf.Alaska.edu.
Umpierre, M., Halpern, M., 1971. Edades Rb-Sr en rocas cristalinas del sur de la República Oriental del Uruguay. *Revista de la Asociación Geológica Argentina*, Buenos Aires 26 (2), 133–151.
Vavra, G., Gebauer, D., Schmid, R., Compston, W., 1996. Multiple zircon growth and recrystallization during polyphase Late Carboniferous to Triassic metamorphism in granulites of the Ivrea Zone (Southern Alps): an ion microprobe (SHRIMP) study. Contrib. Mineral. Petrol. 122 (4), 337–358.
Vavra, G., Schmid, R., Gebauer, D., 1999. Internal morphology, habit and U-Th-Pb microanalysis of amphibolite-to-granulite facies zircons: geochronology of the Ivrea Zone (Southern Alps). Contrib. Mineral. Petrol. 134 (4), 380–404.
Vermeesch, P., 2018. IsoplotR: a free and open toolbox for geochronology. Geoscience Frontiers 9 (5), 1479–1493.
Wayne, D.M., Sinha, A.K., 1988. Physical and chemical response of zircons to deformation. Contrib. Mineral. Petrol. 98 (1), 109–121.
Williams, I.S., Compston, W., Black, L.P., Ireland, T.R., Foster, J.J., 1984. Unsupported radiogenic Pb in zircon: a cause of anomalously high Pb-Pb, U-Pb and Th-Pb ages. Contrib. Mineral. Petrol. 88 (4), 322–327.